Article

Open-source Hardware Design of Modular Solar DC Nanogrid

Md Motakabbir Rahman , Sara Khan , Joshua M. Pearce *

Posted Date: 2 August 2024

doi: 10.20944/preprints202408.0085.v1

Keywords: photovoltaic; open source; open hardware; microgrid; nanogrid; DC nanogrid; modular PV system hardware; solar energy; renewable energy

Article

Open-Source Hardware Design of Modular Solar DC Nanogrid

Md Motakabbir Rahman [1,2], Sara Khan [2] and Joshua M. Pearce [1,2,3,*]

[1] Department of Electrical & Computer Engineering, Western University, London, ON, Canada.; mrahm339@uwo.ca
[2] FAST lab, Western University, London, ON, Canada.; skha242@uwo.ca
[3] Ivey School of Business, Western University, London, ON, Canada.
* Correspondence: joshua.pearce@uwo.ca

Abstract: The technical feasibility of solar photovoltaic (PV) direct current (DC) nanogrids are well-established, but the components of nanogrids are primarily commercially focused on alternating current (AC)-based systems. Thus, DC converter-based designs at the system level require personnel with high degree of technical knowledge and this results in high costs. To enable a democratization of the technology by reducing the costs this study provides a novel modular plug-and-play open source DC nanogrid. The system can be customized according to consumer requirements, enabling the supply of various voltage levels to accommodate different device voltage needs. The step-by-step design process of the converter, controller, data logger, and assembly of the complete system is provided. A time-domain simulation and stability analysis of the designed system were conducted in MATLAB/Simulink as well as experimental validation. The results show transforming the nanogrid from a distribution network to a device makes it suitable for various user-specific applications, such as remotely supplying power to campsites, emergency vehicles like ambulances, and small houses lacking grid electricity. The modular DC nanogrid includes all the features available in a DC distribution network as well as data logging, which enhances the user experience and promotes the use of solar-powered DC grid systems.

Keywords: photovoltaic; open source; open hardware; microgrid; nanogrid; DC nanogrid; modular PV system hardware; solar energy; renewable energy

1. Introduction

The nanogrid functions as a fundamental unit in any distribution network. Typically, it is referred to as a building block of microgrids, which are systems that integrate multiple conventional power sources and distributed energy resources to supply power over a large area [1]. A microgrid can typically be divided into a network of nanogrids, each serving localized power demands within the smaller area coverage [2]. The difference between microgrids and nanogrid is based on their power supply capability and the range over which they can distribute power. A nanogrid is defined as a standalone DC distribution network that integrates distributed renewable energy resources to supply electricity to a small cluster of loads [3]. To be classified as a nanogrid, the system must meet a power requirement in the range of few watts to 5 kW for residential loads [4]. Based on its power-supplying capability, a nanogrid is suitable for small specific systems, that may be completely isolated from the grid network or may be connected to the grid for uninterruptible power supply.

Solar photovoltaic (PV) systems stand out for their sustainability [5], low-cost [6] effectiveness and reliability[7] among renewable energy options [8]. Solar energy is a promising resource in most tropical regions and areas with extended daylight hours across the globe [9,10]. In addition, recent PV costs declines [11] have made it the lowest-cost source of power in most of the world [12]. Thus, solar DC nanogrid is gaining attention worldwide for meeting electrical demands and is suggested for places where grid electricity remains inaccessible [13]. Solar DC nano grid can save up to 25% of

 doi:10.20944/preprints202408.0085.v1

cost for a specific area in Kutubdia, Bangladesh by eliminating the use of inverters [14]. An analysis of the economics of a solar DC nanogrid in a region of KwaZulu-Natal Province, South Africa [15] and in Nigeria [16] showed that the net cost of energy was significantly lower than that of a diesel generator. In addition, the future of null net energy buildings can be achieved by practically implementing DC nano grid [17]. Small-scale nanogrids are being implemented worldwide, particularly in regions with expensive grid electricity or inadequate grid coverage [18]. The availability of various table-top appliances that directly operate on DC made the implementation of DC nano grid easier and more logical [19]. Those appliances include LED lights, laptops, mobile chargers, television, computers, and even DC-based appliances like refrigerators. Taking advantage of appliances operating directly on DC, the implementation of DC-based homes have been completed in many locations including the US, Indonesia, and Philippines to supply basic household loads at a voltage level of 48V DC [20,21]. In a small DC network, smart sockets along with a communication network were integrated to control and measure all the devices that are connected to the system. From the DC nanogrid setup, substantial power savings (around 30%) was obtained compared to AC [22]. There have been numerous implementations of DC nanogrid systems. For instance, a hybrid nanogrid integrating solar PV, wind turbines, and batteries as distributed energy resources was successfully installed to supply local loads [23]. In addition, a DC nano grid system that was capable of generating and distributing power up to 1.2 kW in a voltage level of 24V was also designed [24]. Furthermore, two DC voltage levels, 380V and 48V, were proposed and experimentally validated for compatibility with conventional AC-powered appliances [25].

So, the feasibility of solar DC nanogrid has already been established, with most of the components of nanogrid being well-defined. The converter technologies, maximum power point tracker (MPPT), and battery charge controller technologies are well-established products that are used in conventional solar PV nanogrid systems. But these systems are designed for use in AC systems, and as a result, DC converter-based designs at the system level require personnel with high technical knowledge for proper design, connection, and integration of all components [26]. They are not readily available in the market for nanogrid use. The hardware implementation of DC nanogrid is challenging for the average user because it requires extensive technical expertise to ensure the safe and proper operation of all components, including converters, controllers, energy storage systems, and monitoring devices [27]. This raises costs and limits wide acceptance of a proven technology.

To address this issue, a novel modular version of the DC nanogrid has been designed here to be installed at consumer premises in device form, operating as a plug-and-play device that can be customized according to consumer requirements. The design follows open hardware best practices to ensure maximum accessibility [28,29]. Earlier, the architecture, controller design, stability analysis, and a novel energy management system (EMS) of modular DC nano grid were proposed [30] and here this paper introduces the first hardware setup of a modular, plug-and-play open source nanogrid device, operable with minimal technical expertise, akin to other consumer electronics available in the market. This modular DC nanogrid can be easily customized according to consumers' power requirements, enabling the supply of various voltage levels to accommodate different device voltage needs. All designs utilize open-source hardware and software, ensuring accessibility for users worldwide. The step-by-step design process of the converter, controller, data logger, and assembly of the complete system is provided. A time-domain simulation and stability analysis of the designed system were conducted in MATLAB/Simulink. Subsequently, the connection and disconnection of a 30W load were observed to assess the stability of the designed hardware. The results are presented and discussed in the context of transforming the nanogrid from a distribution network or system to a device makes it suitable for various user-specific applications, such as remotely supplying power to camp vehicles, campsites, emergency vehicles like ambulances, and small houses lacking grid electricity.

 doi:10.20944/preprints202408.0085.v1

2. Materials and Methods

2.1. System Architecture

In the nanogrid architecture shown in Figure 1, a PV converter connects the PV modules to the DC bus. Additionally, bidirectional battery converters and load converters link lithium-ion (Li-ion) batteries and various loads to the grid. Among the low voltage levels (12V to 100V), 48V is identified as the optimal choice for cost and performance. The nanogrid design is scalable; additional PV modules and interface converters can be added to the bus to increase generation capacity. Similarly, extra batteries can be integrated using additional battery converters to support increased loads or storage needs. The EMS can manage variations in DC load and weather conditions, enhancing the system's modularity and adaptability.

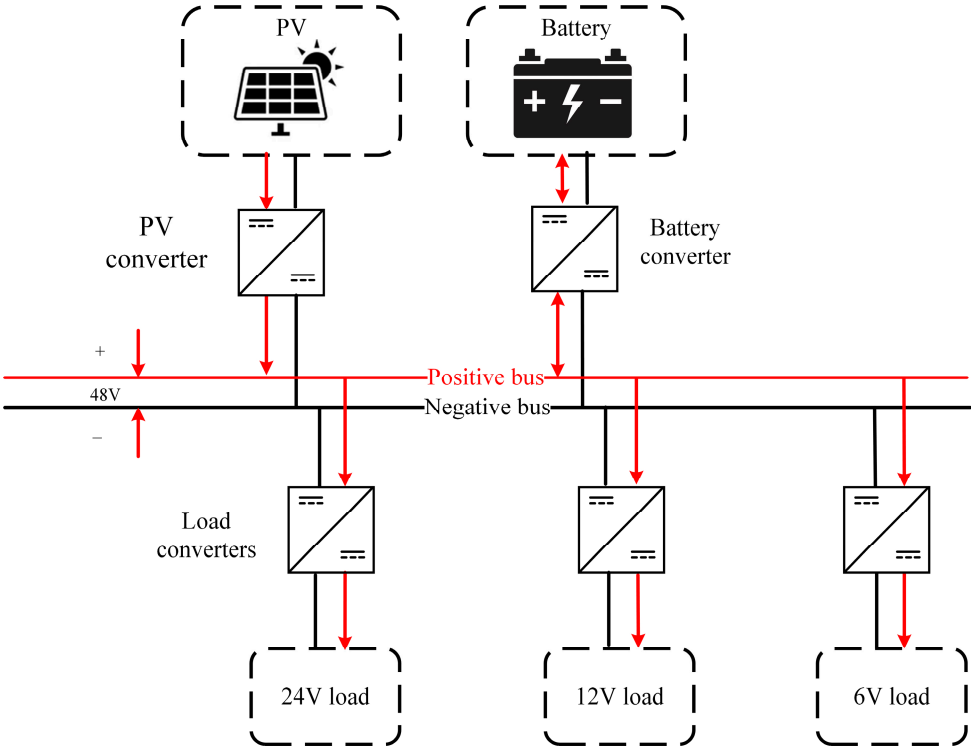

Figure 1. Architecture of DC Nano grid.

In the nanogrid, the battery discharges only in power deficit mode, defined by a bus voltage below 48V. The controller compares the bus voltage to a reference value, initiating battery discharge to raise the bus voltage to 48V. In power surplus mode when bus voltage is above 48V, the controller lowers the bus voltage to reference 48V and initiate battery charging. Three different levels of load can be served using a step-down load converter, and loads rated at 48V can be directly connected to the bus, as the bus voltage remains stable.

2.2. Converter Topology for DC Nano Grid

A nanogrid has the potential to function independently without integrating with the AC grid, but the intermittent nature of renewable energy resources may necessitate connecting the AC grid to the DC distribution network to ensure a continuous power supply. This connection requires an AC/DC converter to link the AC supply to the bus network. The smooth operation of the DC nanogrid largely depends on the stability of the bus voltage. Given the possibility of multiple distributed energy resources being connected to the DC nanogrid, along with battery storage or an external utility grid (or both) for continuous power supply, controlling the bus voltage becomes crucial. This is where

 doi:10.20944/preprints202408.0085.v1

electronic power converters come into play. Power converters act as interfaces for each element connected to the DC bus, each with different roles but ultimately ensuring the stability of the entire nanogrid system. As such, extensive studies are conducted to identify the best architecture for these converters. Various topologies are examined in terms of design, modes of operation, and control mechanisms to optimize the performance and stability of the nanogrid and summarized in Table 1.

Table 1. Comparative analysis of various converter topologies proposed in literatures.

Converter	Interface	Performance	Hardware	Ref.
Two-stage PWM bidirectional converter	Grid to bus	Stabilize the dc bus voltage with minimum ripple and faster dynamic responses. Significant reduction in dc-link capacitor.	Yes	[31]
Switched Boost Inverter (SBI)	Grid to bus	Modified conventional PWM control technique and implemented in digital domain.	Yes	[32]
Cascaded two-stage bidirectional converter	Grid to bus	Featured a Dual Active Bridge (DAB) converter followed by a bidirectional dc-ac converter and operates in three different modes.	Yes	[33]
Two-stage bidirectional grid interface converter (BGIC)	Grid to bus	Efficiency was found greater when first stage converter was controlled by Neutral Point Clamped (NPC) topology and second stage by a full bridge NPC structure.	No	[34]
High-gain bidirectional dc-dc converter	Bus to battery storage	Ensured stability in both grid-connected and islanded modes of the nano grid, reducing voltage ripple, eliminating the chance of improper switching between modes of operation and establishing smooth bidirectional power flow.	No	[35]
Boost derived hybrid converter (BDHC)	Bus to loads	Efficiency is higher than conventional DC nanogrid converter where dedicated converters are required for each component.	Yes	[36]
Fourth-order bidirectional dc-dc converter (FoBiDC)	Bus to battery storage	Exhibited continuous bus side and battery side operation with minimum ripple while minimizing the effect of non-linearity for multiple converter-based system.	Yes	[37]
Bidirectional modular PV battery system (BMPBS)	PV to bus	Problems associated with PV modules like module mismatch, module open circuit due to partial shading were eliminated.	Yes	[38]

2.3. Design of Controllers

The nanogrid controller coordinates various power sources to achieve optimal power flow. The Energy Management System (EMS) proposed in [30] maintains this coordination and dispatches the required power levels demanded by the load. Various control strategies can be implemented, broadly classified into centralized, decentralized, and hybrid control topologies [39].

In the centralized control method, a central controller manages the power, voltage, and load of the nanogrid using data from various sources and loads, communicated through a network, with all units in the nanogrid directly interfacing with the central controller. This central controller makes decisions based on information collected from sensors attached to all sources and loads via communication channels. While this strategy is fast and precise, it has a significant drawback: a single communication link failure can lead to total grid failure [40]. In contrast, the decentralized control scheme has each unit in the nanogrid collect local information from sources or loads through individual sensors. This approach is more robust and reliable as it avoids costly communication links [41]. Coordination between units, fault management, and overall system data monitoring, however, become more challenging [42]. Hybrid distributed control combines elements of both distributed and decentralized control. In the hybrid topology, converters in the nanogrid communicate with each other to create a cohesive control strategy and share information with the central master controller. Local control decisions are made by local controllers, while the central master controller oversees the entire system and makes broader decisions. This approach enhances system reliability by eliminating dependence on a dedicated communication link all the time and makes the system more resistant to failures.

 doi:10.20944/preprints202408.0085.v1

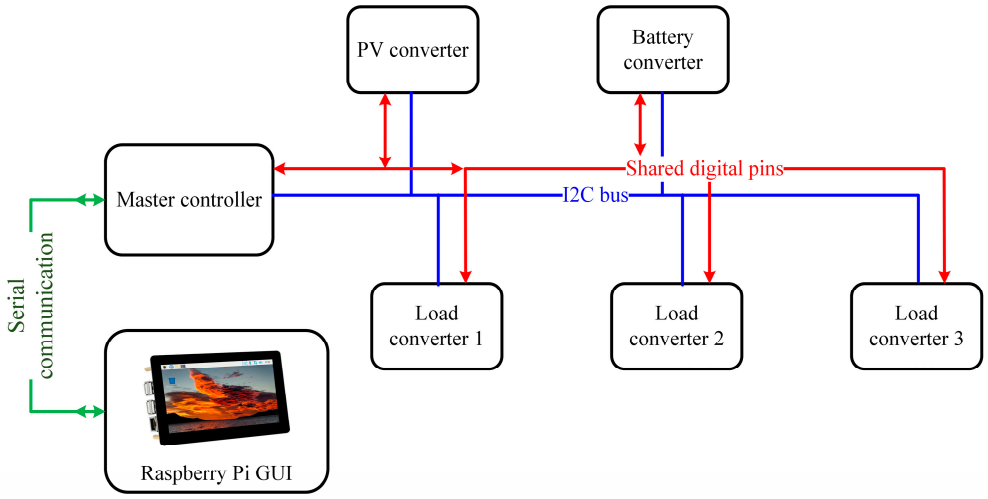

Figure 2. Hybrid control model of modular DC nano grid.

In this modular open-source DC nanogrid system, a hybrid control technique is used to implement the EMS. Converters manage source and load level control, while a dedicated central controller coordinates each unit shown in Figure 1. Communication between the units and the central controller occurs through two methods. Critical information is shared via the digital pins of the Arduino microcontroller, with specific pins dedicated to the PV controller and the battery converter to indicate their modes, and another for the master controller to manage all units. Additionally, the master controller connects to all converters using an I_2C path, allowing the central controller to collect local information cyclically and to interrupt, control, or send commands to each converter as needed [43]. This hybrid approach delivers a powerful and fast control system with enhanced resilience to failure.

2.3.1. PV Controller Design

Based on the battery charging status and state of charge (SOC), the PV controller operates in two different modes. When the battery is in a constant current charging state and connected to the system, the PV controller operates in MPPT mode. In this mode, the controller maximizes the input power from the PV using an MPPT algorithm implemented through PWM control, while the battery regulates the bus voltage. When the battery is nearly charged and in a constant voltage charging state, where the charging current depends only on the battery SOC, or when the battery is fully discharged and the PV is connected to the system, the PV switches to bus control mode. In this mode, the converter maintains the bus voltage at a defined 48V using a PI controller. The schematic diagram of this PV controller is given in Figure 3.

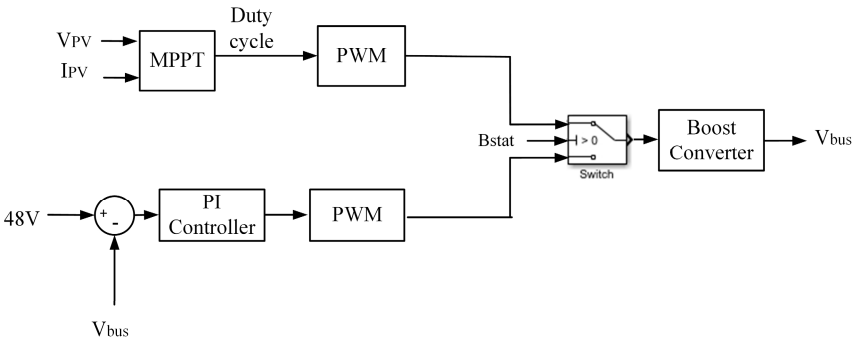

Figure 3. PV controller for boost converter.

 doi:10.20944/preprints202408.0085.v1

Generally, the cost of commercial MPPT devices is significantly higher than solar charge controllers, making them less accessible and affordable for users [44]. Previous work has shown a successful strategy for accelerating innovation and lowering hardware costs is to use an open source design [45,46]. Previous studies have argued open source design should be applied to PV systems and components to reduce costs [47]. Following that theory, to help make small solar PV systems more economically accessible and easier inclusion in the DC bus an efficient MPPT PV converter is designed, in this study a new open source MPPT is designed to reduce the price gap between MPPT and solar charge controllers. There has been some open-source hardware development in the electronics of PV systems [48,49], which began with the design of smart monitoring system for different PV applications and majority of these system used Arduino microcontrollers for conditioning and processing the output signals of the sensors and it was flexible, modular, and scalable, and of low cost [50]. A prototype of an MPPT using the microcontroller PIC16F877A was designed for 10W power, which is very low power and not suitable for most applications or commercial use [51].

Different tracking methods were introduced in the MPPT hardware such as particle swarm optimization (PSO) technique [52] and incremental conductance algorithm [53]. These MPPT methods can be categorized into four groups: conventional, intelligent, optimization, and hybrid techniques [54]. Among the conventional MPPT methods, the variable step size incremental conductance MPPT algorithm automatically adjusts the step size to improve MPPT speed and accuracy. The step size is determined based on the derivative of power to voltage of the PV array [55]. Conventional methods are less effective under partial shading and have slower response times, whereas intelligent, optimization, and hybrid techniques can handle partial shading [56,57]. The optimization methods like PSO [58], Firefly Algorithm (FA), and Ant Colony Optimization (ACO) are best for extracting power from PV under partial shading conditions as they are more accurate, but require expensive hardware [59,60]. Among all these methods, the perturb and observe (P&O) method is the most popular, and widely used, while artificial intelligence-based methods are fast and stable but require digital applications and multiple sensors [61]. Thus, in this design a modified P&O method is used due to less complexity and comparatively faster tracking capability. Many modified versions of P&O have been developed, which use converter duty cycle as the perturbed signal or adaptive perturbation values [62]. The fundamental concept of the P&O algorithm is to adjust the perturbation amplitude according to the present operational conditions. In the case of the PV controller in DC nano grid it takes the PV voltage and current as an input and generates the optimal duty cycle for the converter.

2.3.2. Battery Controller Design for Bidirectional Converter

The battery controller determines the charging and discharging modes based on the bus voltage and the SOC of the battery. Any surplus energy in the grid increases the bus voltage, indicating a charging state, and vice versa. The SOC or battery voltage indicates the charging state. Depending on this, the battery can be charged in constant current mode or constant voltage mode, as shown in Figure 4.

 doi:10.20944/preprints202408.0085.v1

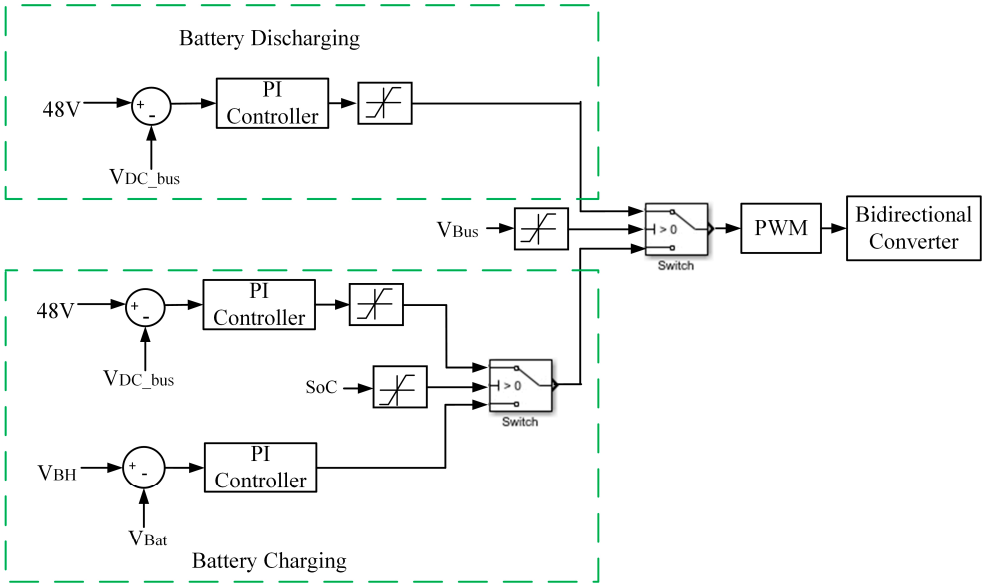

Figure 4. Battery controller.

2.3.3. Load Controller Design

The load controller regulates the output voltage to a specific level using a PI controller. The controller compares the reference voltage with the actual output voltage and adjusts the duty cycle accordingly shown in Figure 5. Additionally, the load controller can disconnect any load upon receiving instructions from the master controller, based on the priority of the specific load.

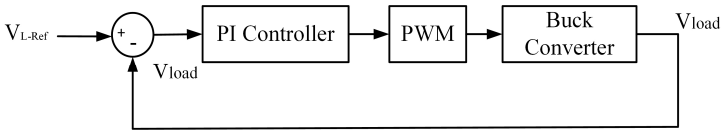

Figure 5. Load controller.

2.4. Converter Design

Three different converter topologies are used in this research to design the modular DC nano grid system with a bus voltage of 48V. The boost converter topology is utilized as the PV converter, with the maximum PV input voltage kept below 48V, preferably between 15-40V. The maximum charging current capacity is chosen to be 16.66A, allowing for the connection of up to 800W of PV panels to the system using a single boost converter module. Multiple such modules can be used in a single system to scale up the PV power.

For charging and discharging the battery, a bidirectional buck-boost converter topology is employed, with the battery voltage considered to be 24V. Given that the lower voltage side is the battery side and allowing a maximum current of 16.67A, up to 400W of power can be charged or discharged using a single battery module in the system.

Lastly, a buck converter topology is used for loads of 24V, 12V, and 6V, with each rated for a maximum of 400W, 200W, and 100W, respectively, within the system. Ensuring that the bus voltage is stable at 48V allows for loads rated at 48V to be connected directly to the bus without any intermediary converters. The specifications of these modules, along with the PV, battery, and load ratings, are included in Table 2.

 doi:10.20944/preprints202408.0085.v1

Table 2. System specifications.

Parameters	PV module	Battery module	Load module
Converter type	Boost converter	Bidirectional converter	Buck converter
Converter power rating (W)	800W	400W	400W (24V), 200W (12V), and 100W (6V)
Input voltage range (V)	15-40V	20-29.4 V (24V battery)	48V
Maximum input current (A)	20A	16.67A	(8.33 A, 4.17 A, 2.08 A)
Output current (V, A)	16.67A	8.33A	16.67A

The components of the converter and the controller parameters are calculated and listed in Table 3. Components are chosen to exceed their critical ratings and are matched to the nearest common inductor and capacitor values. Based on these parameters, an open-source hardware nanogrid is designed and licensed under GNU GPL v3, CERN OHL v2, and OSF. All code, GUI, 3D-printed parts, and converter PCBs are uploaded to an open-source repository [63].

Table 3. Converter components and controller parameters calculation.

Parameter	Boost Converter	Bidirectional converter	Buck converter (24V)	Buck converter (12V)	Buck converter (6V)
Critical Inductance	L_1=45 µH	L_2= 115.2 µH	L_3=57.58 µH	L_4=43.18 µH	L_5=25.2 µH
Critical Capacitance	C_1= 260 µF	C_2= 217.01 µF, C_3= 173.6 µF	C_4= 43.41 µF	C_5= 86.83 µF	C_6= 173.61 µF
Selected Inductance	L_1=47 µH (20A)	L_2= 120 µH (16.67A)	L_3=68 µH (16.67A)	L_4=47 µH (16.67A)	L_5=33 µH (16.67A)
Selected Capacitance	C_1= 470 µF (100V)	C_2= 470 µF (50V) C_3= 470 µF (100V)	C_4= 470 µF (50V)	C_5= 470 µF (50V)	C_6= 470 µF (50V)
Proportional gain (Kp)	0.00021	Charging mode: 0.0004 Discharging mode: 0.0005	0.000451	0.000722	0.00021
Integral gain (Ki)	2.734	Charging mode: 4.78 Discharging mode: 6.01	9.52	11.01	9.35
Gain Margin (GM)	15.57dB	17.32dB, 15.3dB	14.18 dB	20.8 dB	13.85 dB
Phase Margin (PM)	90^0	90^0 ,90^0	90^0	90^0	90^0

2.4.1. Bidirectional Battery Converter Design

The bidirectional buck-boost converter is designed using two alternately switched MOSFETs and one reverse parallel diode to reduce stress on the lower-side MOSFET when it is switched off. The duty ratio of the switching pulse is controlled to regulate both the current and the direction of current flow. With the battery connected to the source terminal of the high-side MOSFET, an IR 2104 MOSFET driver with a bootstrap capacitor keeps the gate voltage above the battery voltage during switching. The Arduino Nano manages the switching pulse and controls the charging and discharging current by monitoring four parameters: battery voltage, charging current, bus voltage, and discharge current, all through a 16-bit ADS1115 analog-to-digital converter. The ADC can have four unique addresses, which allows multiple battery converters to be connected and share data using the same I_2C bus.

The Arduino code limits the discharge current to the maximum allowable battery discharge rate. During charging, two modes are utilized for the lithium battery until the state of charge (SOC) reaches 95%. Initially, the controller charges the battery at the current supplied by the MPPT, provided it is below the maximum charging current of the battery. Once the SOC is 95%, the charging mode switches to constant voltage mode, charging the battery at a constant voltage with lower current. At this point, the digital pin dedicated to the battery controller (BS) is set high, signaling the MPPT to switch from MPPT mode to bus control mode. The schematic and PCB of the bidirectional converter is shown in Figure 6. The assembled battery converter with components on the board are shown in Figure 7.

 doi:10.20944/preprints202408.0085.v1

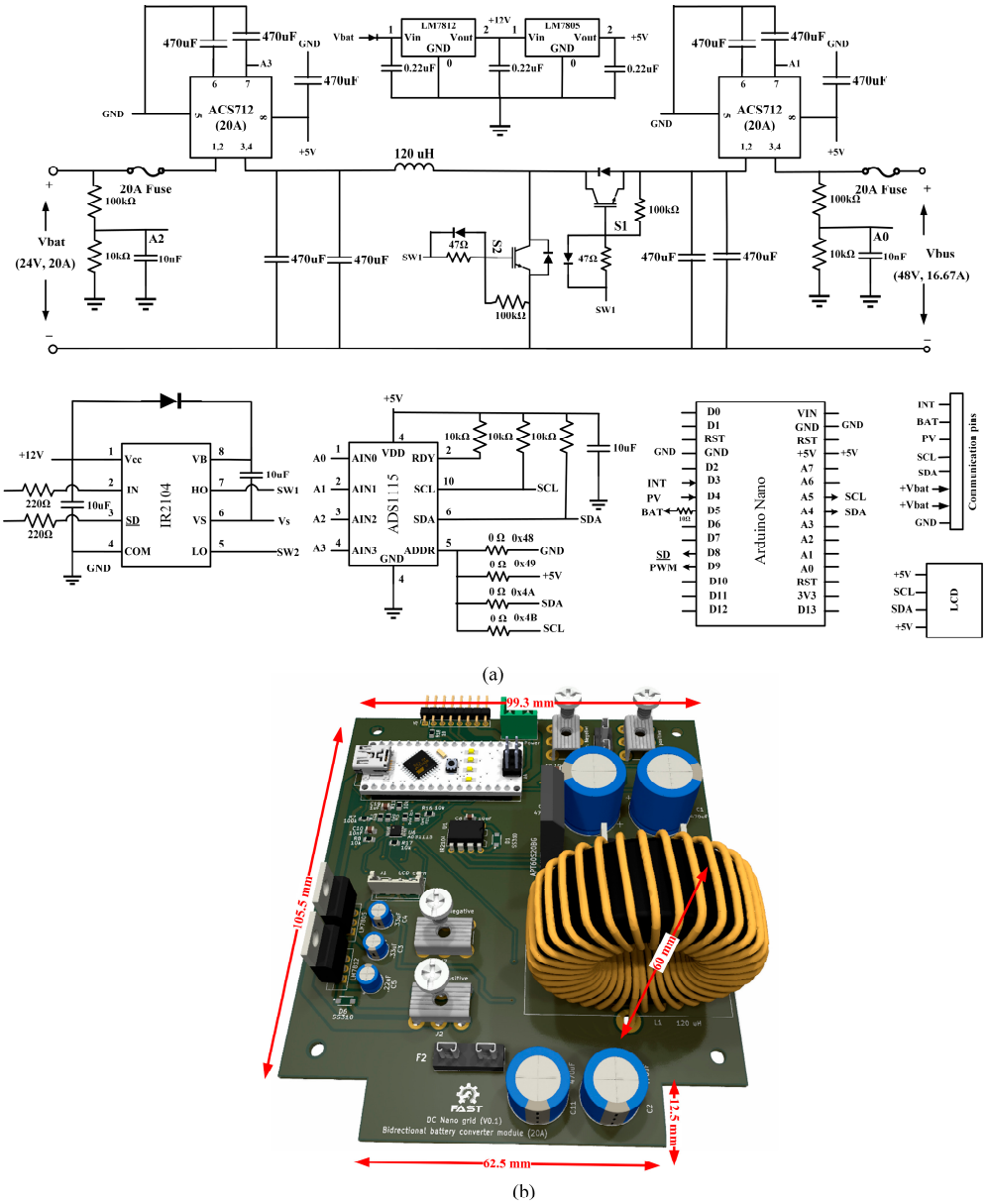

(a)

(b)

Figure 6. (a) Schematic of bidirectional converter for battery, (b) 3D assembled PCB of bidirectional converter.

 doi:10.20944/preprints202408.0085.v1

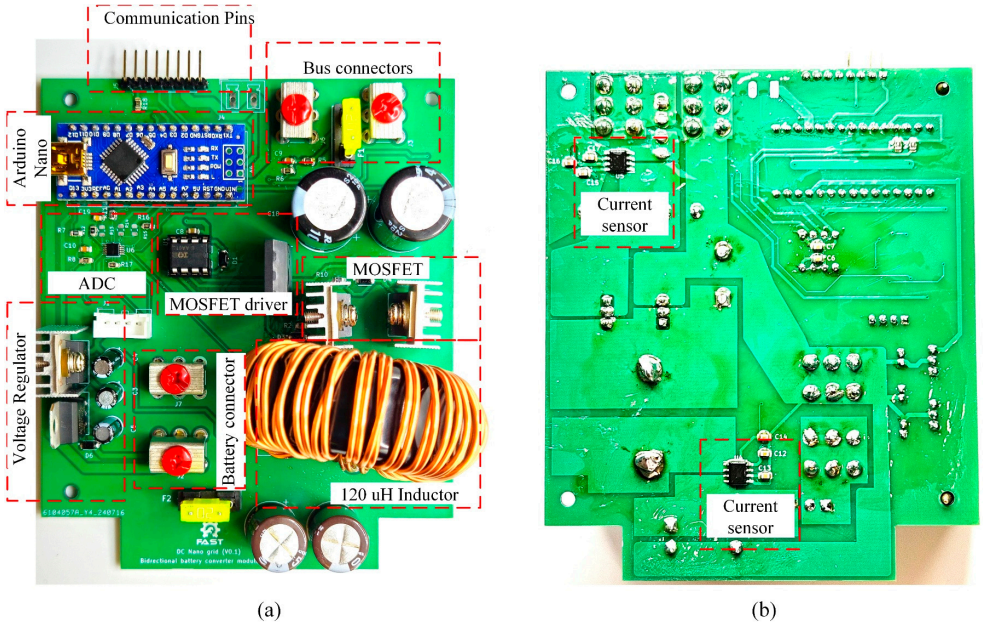

Figure 7. Assembled bidirectional battery converter (a) front side (b) back side.

2.4.2. PV Boost Converter Design

The boost converter for the PV system is rated at 800W, with an input voltage range of 15-40V, and it boosts the voltage to 48V. The converter is designed with one low-side MOSFET and a diode to allow current flow from the PV to the bus. The pulse generated by the Arduino Nano is sufficient to drive the MOSFET. The system measures PV voltage, PV current, bus voltage, and current supplied to the bus using an ADS1115 16-bit ADC. The ADS1115 has four unique addresses, allowing multiple PV and battery converters to connect, each with a unique ADC address, as they all share the same I2C bus. Jumper resistor connections (R13, R15, R14, and R12) provide the four unique addresses of 0x48, 0x49, 0x4A, and 0x4B shown in Figure 8. The PV converter can be excluded from the I2C bus to prevent frequent interruptions by the master controller for data acquisition as they are jumper resistor to isolate from the I2C bus. Instead, an OLED display can be connected to the PV converter to show local vital information, while overall critical system status is shared through the digital pin.

The PV converter operates in two different modes based on the BS signal provided by the battery. When the battery is in constant current (CC) mode, the PV operates in MPPT mode. The rest of the time, it operates in bus control mode. The components and the assembled boost converter are shown in Figure 9.

 doi:10.20944/preprints202408.0085.v1

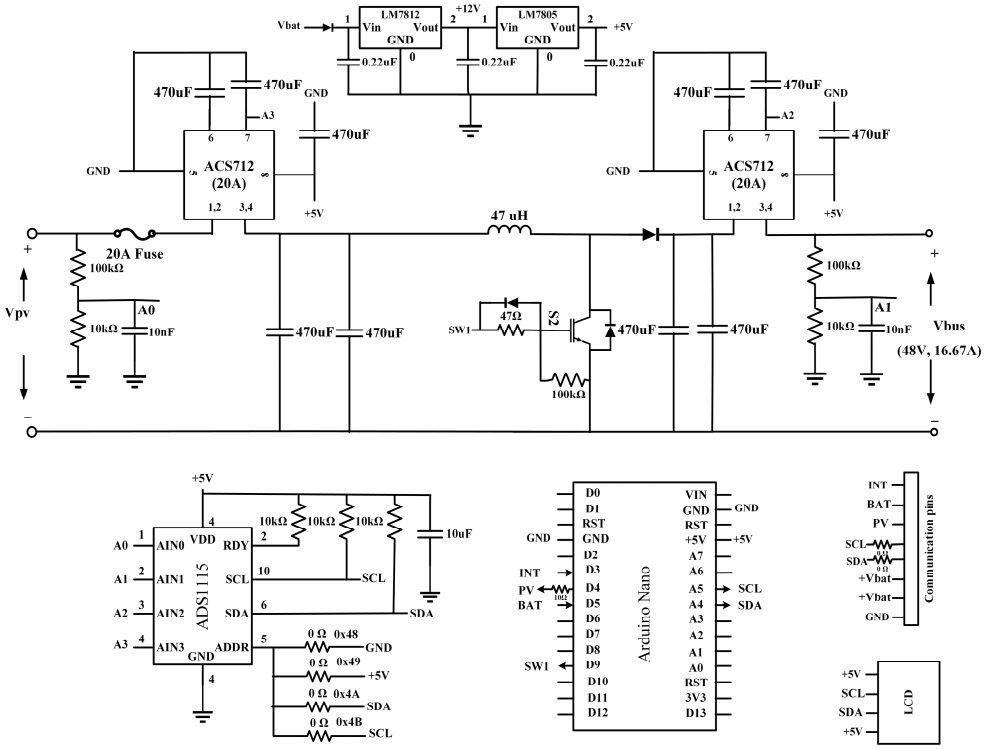

(a)

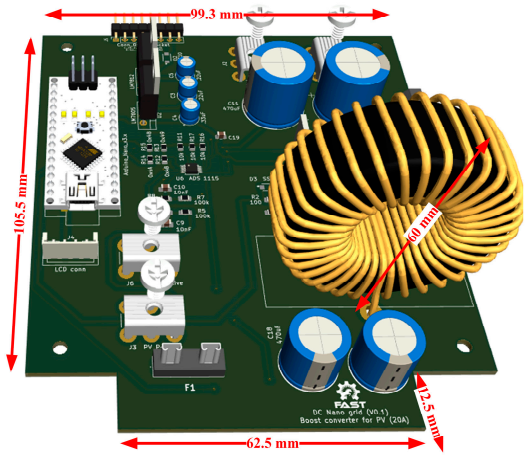

(b)

Figure 8. (a) Schematic of boost converter for PV, (b) 3D assembled PCB of boost converter.

 doi:10.20944/preprints202408.0085.v1

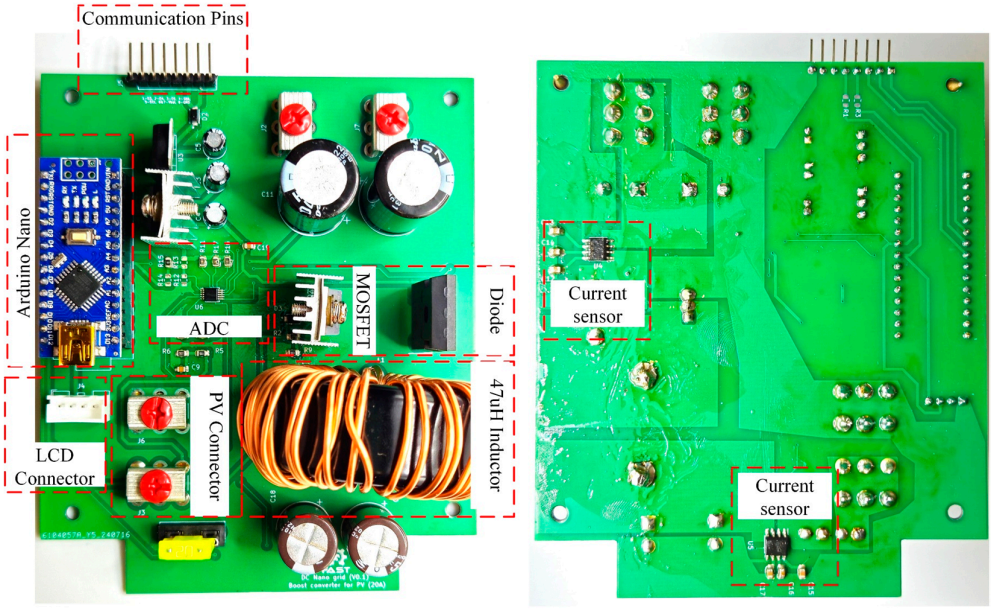

Figure 9. Assembled boost converter for PV (a) front side (b) back side.

2.4.3. Buck Converter Design

To serve loads of different voltage levels, a DC-DC converter was designed using an open-source Arduino Nano and a PI controller to regulate the output voltage according to a predefined reference. This converter is a synchronous buck converter utilizing CSD19533KCS MOSFETs (100V,100A) [64] as switches. The IR2104 MOSFET driver IC provides complementary pulse width modulation (PWM) pulses to both the low-side and high-side MOSFETs, with a 10µF bootstrap capacitor included in the driver circuit.

Three different voltage level load converters can be implemented using the same PCB, requiring only the specific inductor for each converter level as previously calculated. Additionally, the master controller can stop the buck converter from supplying the load either by sending a signal through I_2C or by raising the INT pin high. The Buck converter schematic and 3D rendering are shown in Figure 10 and the PCBs are shown in Figure 11.

 doi:10.20944/preprints202408.0085.v1

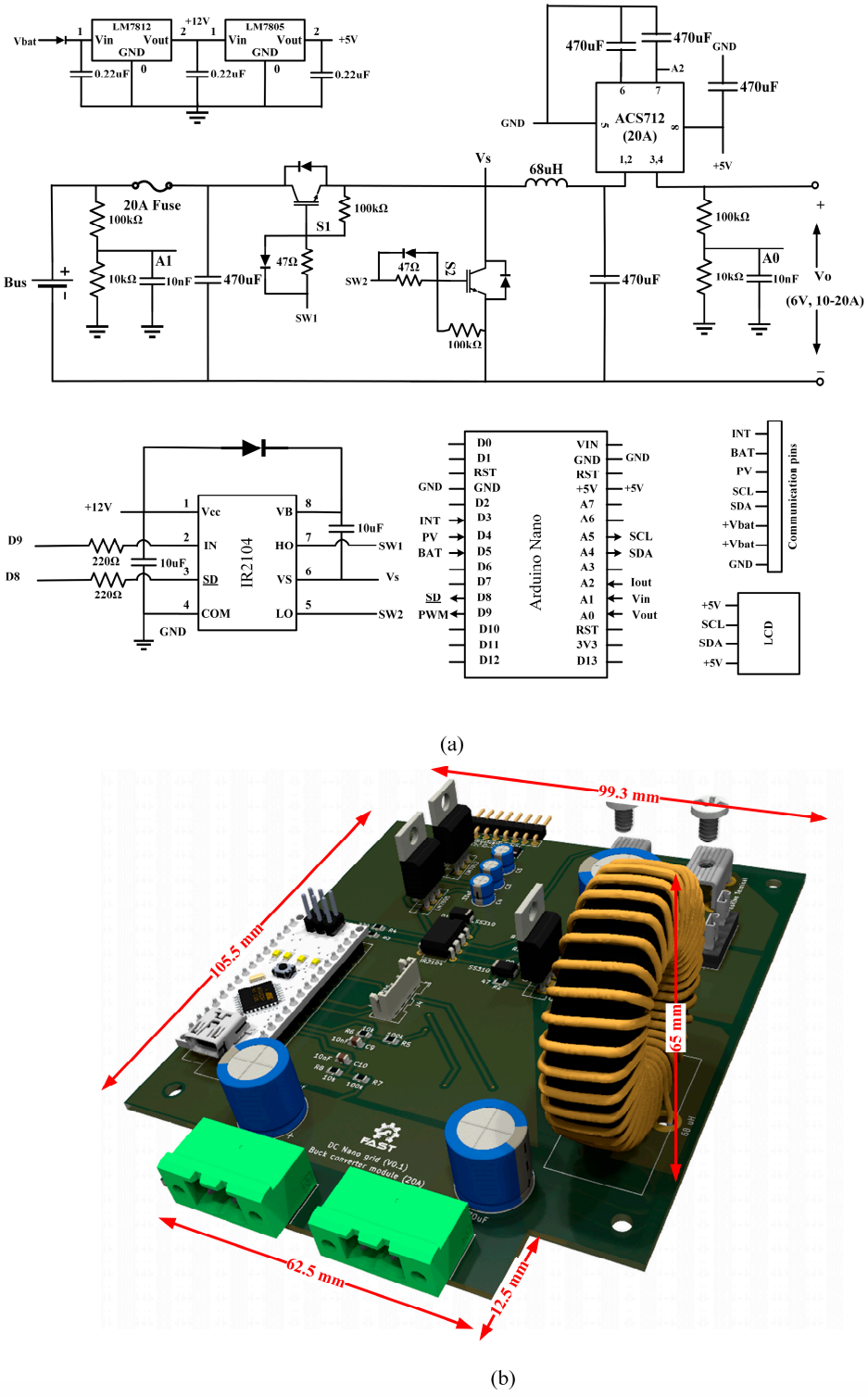

(a)

(b)

Figure 10. (a) Schematic of buck converter for 24V load, (b) 3D assembled PCB of buck converter.

 doi:10.20944/preprints202408.0085.v1

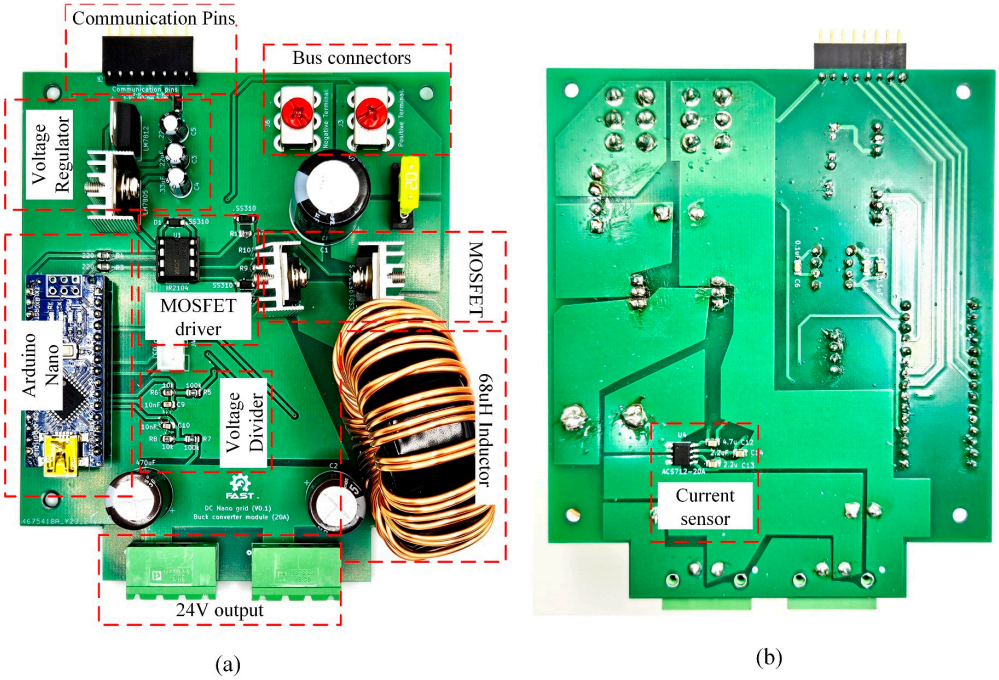

Figure 11. Buck converter PCB with components (a) front side (b) back side.

2.4.4. Master Controller Design

In the nanogrid system, all converters and the master controller share the same I2C bus. The PV and battery converters both use ADS1115 ADCs, communicating over this shared bus. For the PV converter, which continuously monitors current and voltage while adjusting the switch pulse, it can be isolated from this I2C communication without interrupting its operation and display its status on an OLED. Similarly, the battery converter can be isolated with an OLED display connected to it. However, in this project, the battery converter, load converter, and master controller share the I2C bus, with the PV converter displaying its status on its own OLED.

The shared digital pins are always connected to each converter to change their mode of operation. The master controller simultaneously requests voltage, current, and battery SOC data from the battery and load converters. The corresponding converters send back the data, which the master controller then combines sequentially and serially prints to the Raspberry Pi-based GUI and data logger. The circuit and the PCB design of the master controller is shown in Figures 12 and 13.

 doi:10.20944/preprints202408.0085.v1

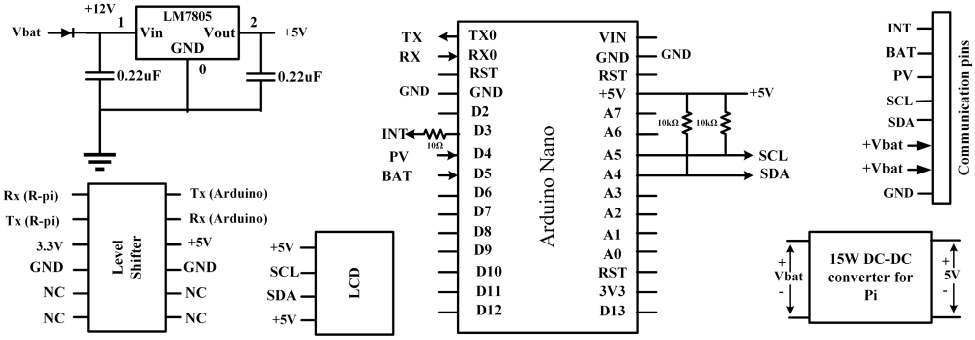

(a)

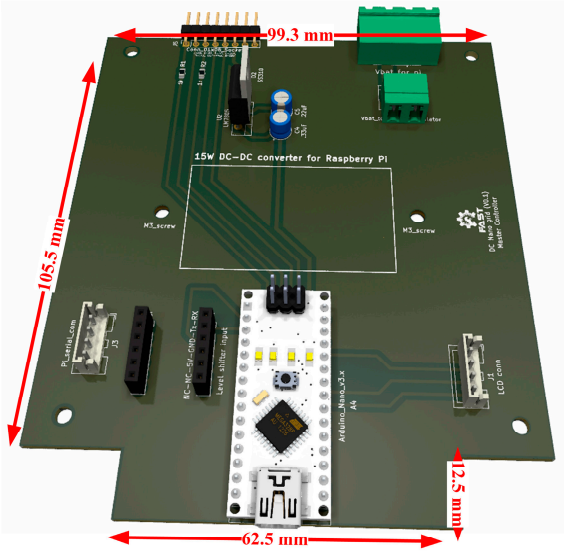

(b)

Figure 12. (a) Schematic of Master controller, (b) 3D assembled PCB of master controller.

 doi:10.20944/preprints202408.0085.v1

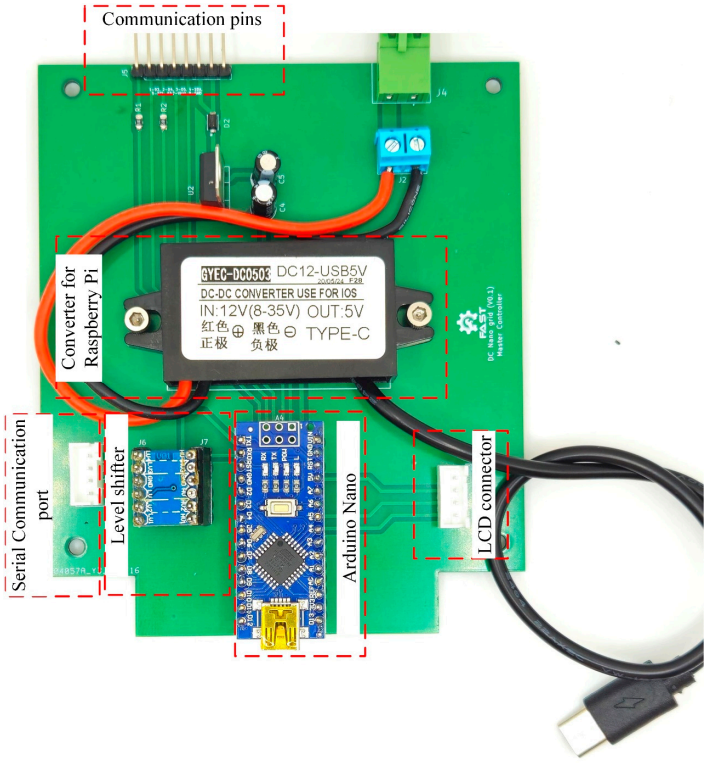

Figure 13. Master controller PCB layout and assembly.

2.4.5. Communication Bus

The communication bus comprises 8 lines used for I2C communication, shared digital pins, and power supply (+12V, GND) shown in Figure 14. It features an 8-pin socket to interface with the pin headers of the converters and master controller, facilitating information exchange among the converters and the master controller. The bus is 25mm in height and is placed inside the DIN rail where the converters communication pins clip in. Pin sockets are spaced 35mm apart, and two communication buses can be interconnected to cover the full length of the DIN rail shown in Figure 15.

Table 4. Function of each traced in the communication bus.

Serial	Trace name	Function
1	PVS (D3)	PV signal from PV converter to indicate operating mode (0=MPPT, 1=Bus control)
2	BS (D4)	Battery status signal from Battery converter (0=Current control, 1=Voltage control/isolated)
3	INT (D5)	Interrupt signal by master (Normally 0)
4	SDA	Serial data line
5	SCL	Serial clock line
6	+12V	+12V supply for the control circuit
7	+12V	+12V supply for the control circuit
8	GND	Common ground

Preprints.org (www.preprints.org) | NOT PEER-REVIEWED | Posted: 2 August 2024 doi:10.20944/preprints202408.0085.v1

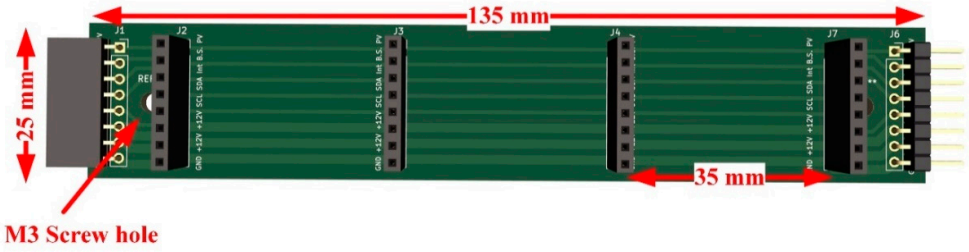

Figure 14. Schematic of Communication bus.

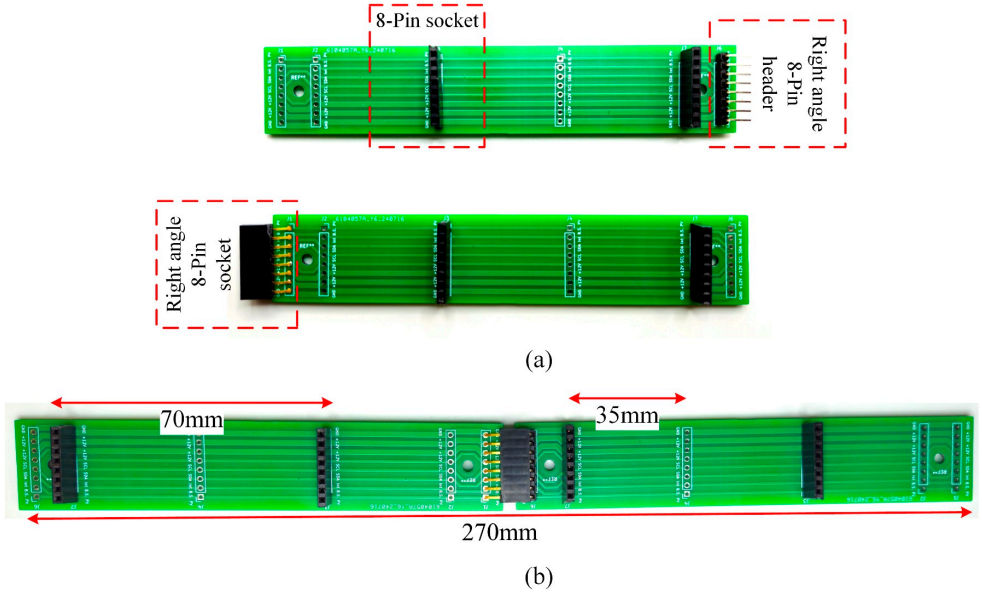

Figure 15. Assembled and extended communication bus.

2.4.6. Inductor Design

For designing the inductors of various converters, each handling a peak current of approximately 20-24A, the toroidal inductor core 0077443A7 from Magnetics (Pittsburgh, PA, USA) is used. This core has an outer diameter of 46.74 mm and a width of 18.03 mm, with a relative magnetic permeability of 75 and an inductance factor of 169 nH per turn. The design parameters for the 47 µH, 120 µH, and 68 µH inductors are summarized in Table 5.

Table 5. Design parameters of inductors.

Parameters	Boost converter	Bidirectional converter	Buck Converter 1 (24 V)
Inductor	L1=47 µH	L_2= 120 µH	L_3=68 µH
Current	20A	16.67A	16.67A
Peak current	24	20	20
Wire AWG	16AWG	16AWG	16AWG
Number of strands	2	2	2
Turns	23	37	28
Length	3,223 mm	5,266 mm	3,924 mm

 doi:10.20944/preprints202408.0085.v1

2.5. Bill of Materials

The bill of materials for all subcomponents is listed in Appendix A. The summary of the total cost for each subsystem is shown in Table 6 and the total cost of the system is CAD$379.

Table 6. Summary of total cost of the system.

Type	Cost (CAD)
Buck Converter	$55.81
Boost converter	$66.07
Bidirectional converter	$76.28
Master Controller	$28.78
Communication Bus	$5.03
Monitoring system	$147.52
Total	$379.49

2.6. Arduino Codes and GUI

Each converter and the master Arduino have separate code, as detailed in Table 7. In addition to the preinstalled libraries in the Arduino IDE, the SSD1306 library for the OLED display and the ADS1115 library for the 16-bit ADC also need to be installed. To avoid interruption from the ADC and OLED display, the firmware must be uploaded to the Arduino before it is placed on the board for the first time. Each converter is assigned a different slave address, defined in the wire setup before initiating transmission, to communicate with the master. If more than one converter of the same type is present in the system, each must be assigned a different wire address.

Table 7. Arduino codes and GUI of the DC nano grid system are all licensed with GNU GPL v3.

Code	File type	Location of file
Boost converter code	.ino	https://osf.io/73yf5/
Buck converter code	.ino	https://osf.io/73yf5/
Bidirectional converter code	.ino	https://osf.io/73yf5/
Master controller code	.ino	https://osf.io/73yf5/
GUI for Raspberry pi	.py	https://osf.io/73yf5/

2.7. Integration of Converters

To house the converters and to interconnect them, an open-source frame is designed to facilitate modular plugging of the converters onto the frame's DIN rail. A display with a Raspberry Pi is used for data monitoring and logging. The converters and the master controller are also housed in individual enclosures. Both the converters and the frame support the installation of the system.

2.7.1. DC Nano Grid Frame Design

The parts required for assembling the frame are listed in Table 8 along with the open-source repository of the files. All custom components can be 3-D printed on a RepRap class-[65,66] open source 3-D printer. Components were printed using polylactic acid (PLA) filament in Prusa MK3 print using print settings given in Table 9.

Table 8. 3D printed parts required for assembly of the frame of the DC nano grid all licensed with CERN OHL-S 2.0.

Parts name	Quantity	File type	Location of file
Sliding corner bracket	8	STEP/stl	https://osf.io/73yf5/
Corner bracket	8	STEP/stl	https://osf.io/73yf5/
Holder for DIN rail	2	STEP/stl	https://osf.io/73yf5/

 doi:10.20944/preprints202408.0085.v1

Holder for bus bar	2	STEP/stl	https://osf.io/73yf5/
Case for display	1	STEP/stl	https://osf.io/73yf5/
Encloser for Raspberry pi	1	STEP/stl	https://osf.io/73yf5/
Raspberry pi holder	1	STEP/stl	https://osf.io/73yf5/

The printing parameters are summarized in Table 9 and can be printed on any RepRap class 3-D printer.

Table 9. 3-D printing parameters.

Parameter	Value
Filament	PLA
Layer Height	0.3 mm
Initial Layer Height	0.2 mm
Infill Density	15 %
Printing Temperature	210 ˚C
Build Plate Temperature	60 ˚C
Print Speed	60 mm/s
Travel Speed	175 mm/s

The frame is designed as an alternative to placing all components inside an electrical box. The parts needed are shown in Figure 16. It will hold three converters and a master controller box, with dimensions of 420mm in length and 390mm in height. These dimensions can be adjusted as needed. Two pieces of 350mm aluminum extrusion bars serve as stands. To support them, three pieces of 80mm long aluminum extrusion are used per stand, totaling six pieces. A 420mm long aluminum extrusion bar connects the two stands together. Two 410mm bus bars cut from a 1m long bus bar. And a 410mm long DIN rail to accommodate the converters. Four types of corner brackets and holders are used in this design process, as detailed in Table 8, also the design steps are mentioned in Figure 17. A case and holder are also made for the display connected to the Raspberry Pi 4b for data monitoring and connected to one of the bars of the frame.

To assemble the frame for accommodating the DIN rail, bus bars, and monitoring system, following steps are followed:

- The stands were assembled using the 350mm aluminum extrusions and 80mm support pieces first.
- The 420mm aluminum extrusion was attached to the stands to form the frame.
- The 410mm bus bars and DIN rail were installed within the frame.
- A case and holder for the display connected to the Raspberry Pi 4b for data monitoring were created and attached to one of the bars of the frame.

Figure 17(a–g) provide detailed design steps and the types of corner brackets and holders used and Figure 18 shows the assembled frame.

 doi:10.20944/preprints202408.0085.v1

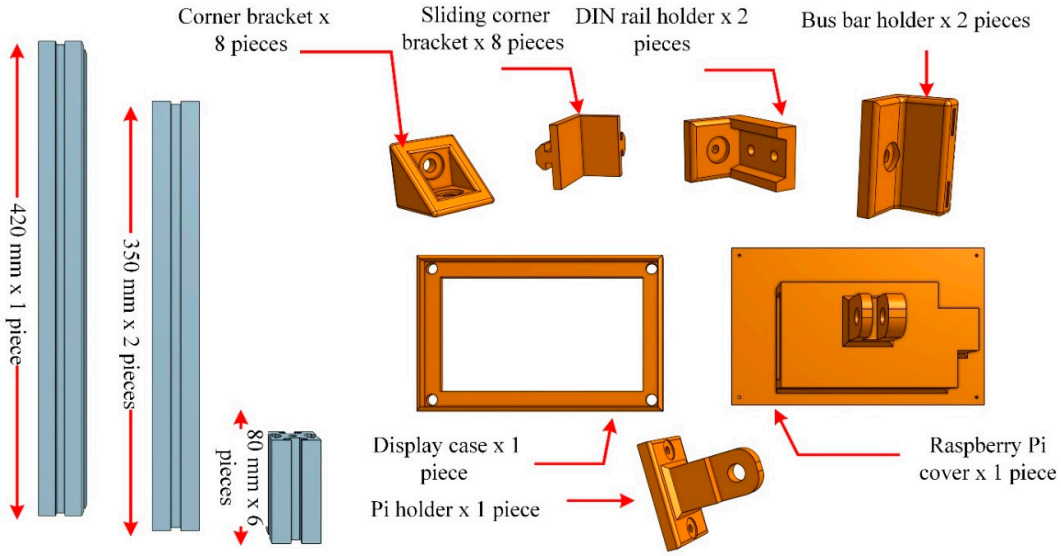

Figure 16. Parts required for assembly of frame.

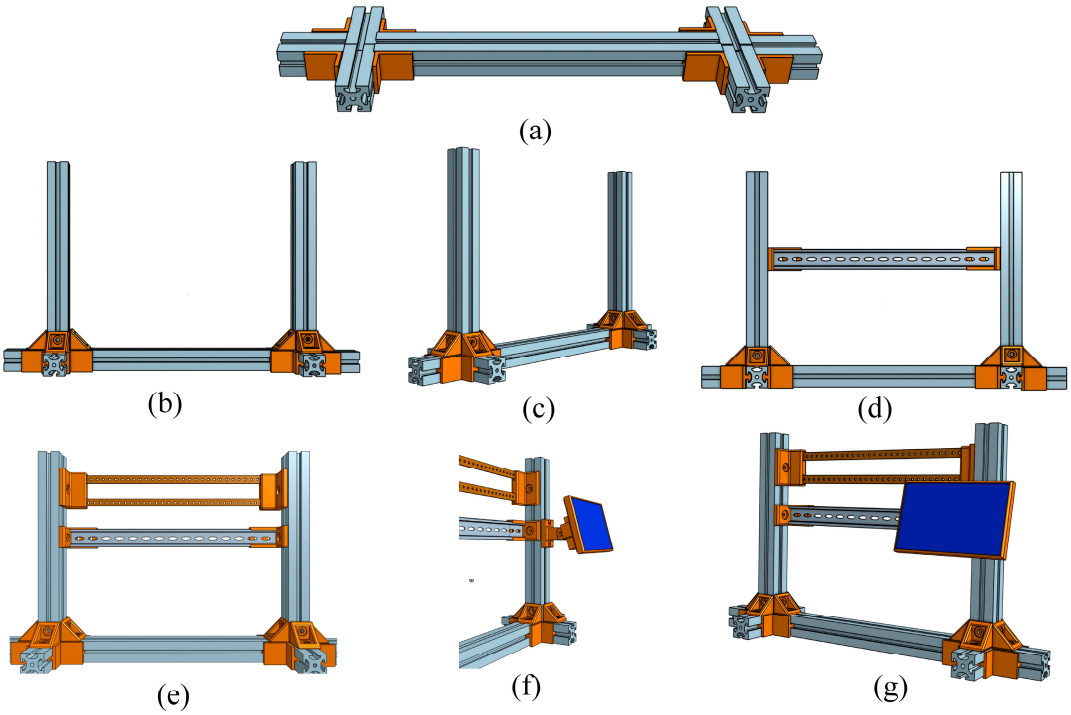

Figure 17. Assembly process of the frame.

 doi:10.20944/preprints202408.0085.v1

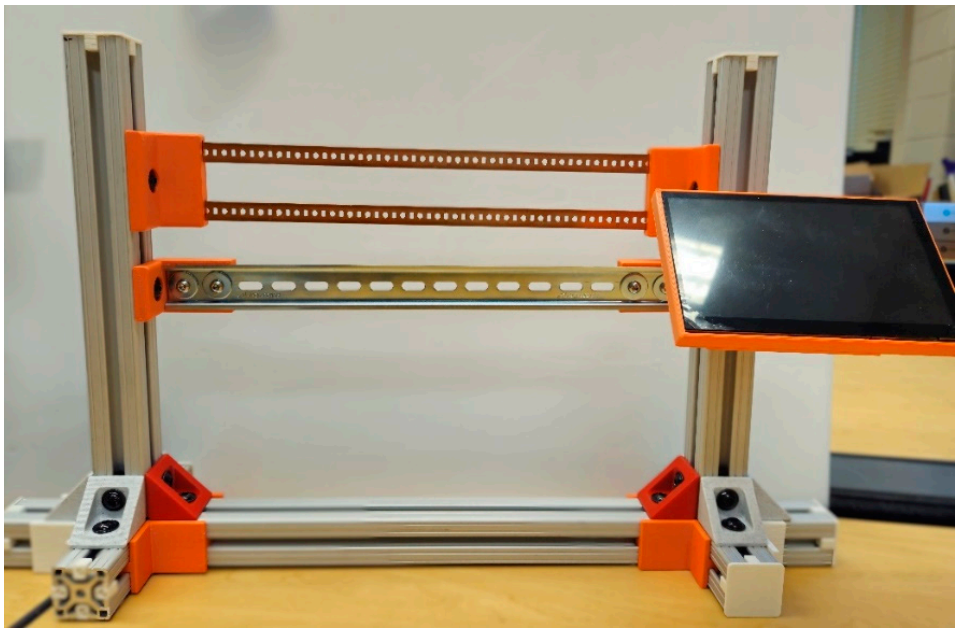

Figure 18. Assembled frame.

2.7.2. Converters Encloser Design

Each converter and master controller have an enclosure that is adequately ventilated. The enclosures are designed with the same shape, but their widths vary based on the converter module, as not all converters have the same width or features. Each module has a clip to connect to the DIN rail, with pockets for passing wires to the bus bar and communication ports. The front panel of the enclosure features different elements based on the module: the Boost converter has its own display, and the master controller has a port to connect the USB from the Raspberry Pi for serial data sharing and power supply. The STEP and STL files for all the enclosures are available in the repository listed in the following Table 10. Rendered images of the master controller are shown in Figure 19. All the enclosures were printed using a 0.6mm nozzle at a 0.3mm layer height with 15% infill, utilizing PLA filament.

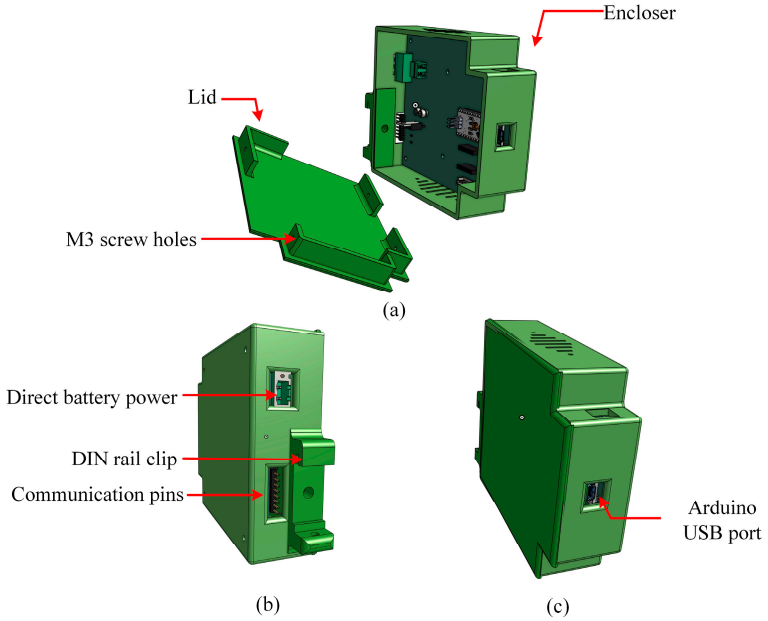

 doi:10.20944/preprints202408.0085.v1

Figure 19. Rendered 3D image of master controller encloser.

Table 10. 3D printed parts required for assembly of converters and master controller all licensed with CERN OHL-S 2.0.

Parts name	Quantity	File type	Location of file
Buck converter encloser	1	STEP/stl	https://osf.io/73yf5/
Buck converter lid	1	STEP/stl	https://osf.io/73yf5/
Boost converter encloser	1	STEP/stl	https://osf.io/73yf5/
Boost converter lid	1	STEP/stl	https://osf.io/73yf5/
Bidirectional converter encloser	1	STEP/stl	https://osf.io/73yf5/
Bidirectional converter lid	1	STEP/stl	https://osf.io/73yf5/
Master controller encloser	1	STEP/stl	https://osf.io/73yf5/
Master controller lid	1	STEP/stl	https://osf.io/73yf5/

2.7.3. Final assembly

After the enclosures are printed, the PCBs are placed inside, and the wiring is completed, the communication pins are attached to the communication bus in all the converters before placing them on the DIN rail. Once the converters are secured in the DIN rails, the necessary connections between all the positive and negative terminals of the converters and the corresponding bus bar are made. The battery converter also has a direct battery power supply port to the master, designated for the Raspberry Pi converter. After all the interconnections are completed, the power supply and USB connection between the master Arduino and Raspberry Pi are established shown in Figure 20.

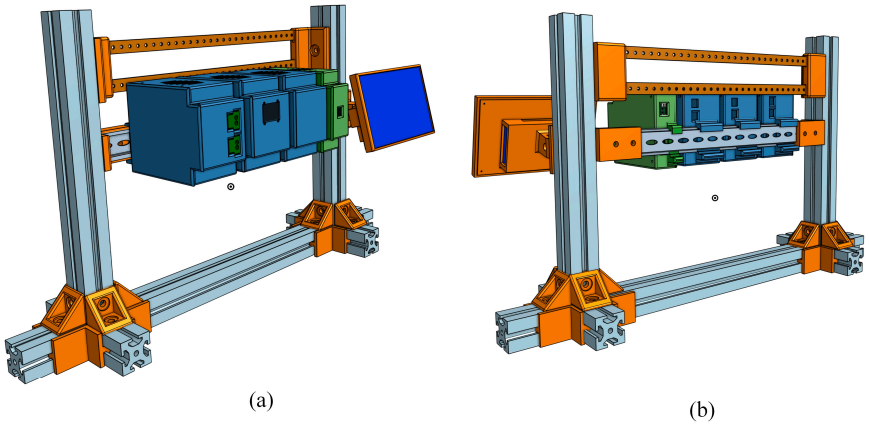

Figure 20. Final assembly rendered 3D image of Nano grid.

2.8. Interface and GUI

All converter controllers utilize Arduino Nano processors, and the EMS also implemented on an Arduino Nano serving as the master processor. This master processor communicates with the other Arduino Nanos within the DC nano grid using an I_2C communication protocol while the master controller only communicates with Raspberry Pi using serial communication protocol. To display the status and voltage/current levels of each converter, a Raspberry Pi (Cambridge, England) with a 7-inch display has been integrated into the system as a separate module. This display module, along with the master Arduino, functions as the central control unit of the entire DC nano grid.

The graphical user interface (GUI) for the DC nanogrid was developed using Python and the Tkinter library shown in Figure 21. Currently, with only the battery converter and one load converter connected, the GUI is designed to display their statuses exclusively. This GUI is open source and can be modified as needed. The Python code acquires serial data sent by the master Arduino, processes it, and displays the information in the corresponding sections. As this is the initial version of the GUI,

 doi:10.20944/preprints202408.0085.v1

it can be easily modified in the future to send commands to the master Arduino for controlling the DC nanogrid.

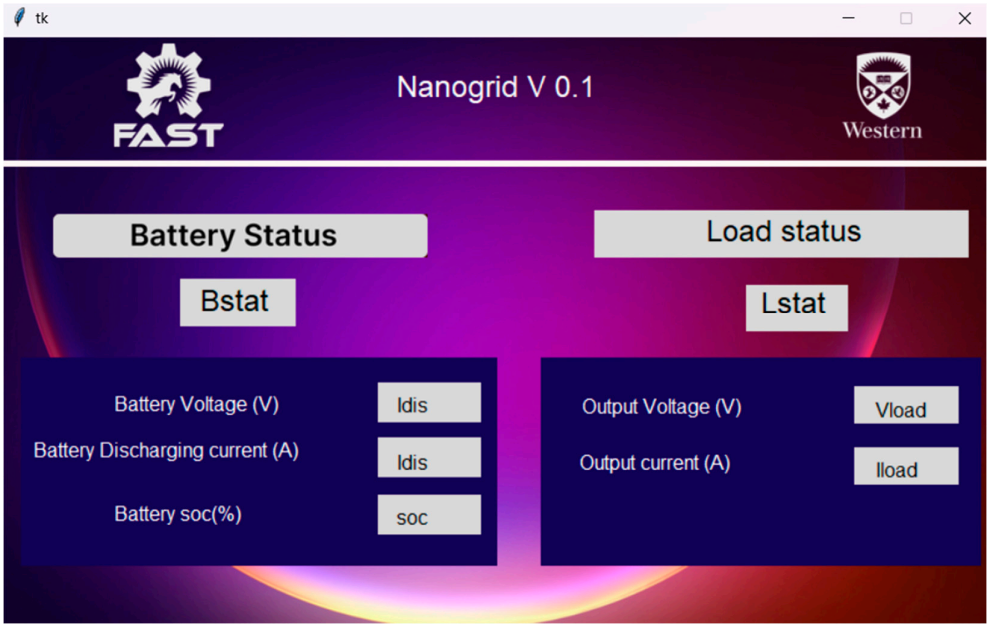

Figure 21. DC nano grid GUI for data monitoring.

2.8. Step by Step Integration and Commissioning Process

The installation process and guidelines are as follows:

- Attach the master controller to the frame. This is the only unit that does not require connections to the bus bar, and there should only be one master controller present in a DC nano grid.
- Attach the PV and battery modules to the system one by one. For systems with multiple PV and battery modules, alternate the installation sequence between PV and battery to maintain consistent DC resistance across all modules.
- Attach the buck converter module and inverters module (if any) to the system according to the load requirements.
- Sequentially turn on all the battery switches. This action will power on the master controller and all connected modules along with the Raspberry Pi display. Next, connect the PV panels to the PV converter, and finally, connect the loads to the system.
- For shutdown, follow the reverse order of the installation process.

3. Results

3.1. MATLAB Simulink Results

To verify the performance of the EMS and stability of the nanogrid by simulation, two different cases were analyzed: (1) variation in PV generation, (2) variation in load.

Case 1: Variation in irradiance

In case 1, the nanogrid operates under varying irradiance conditions which causes variations in the PV generation. Initially the solar irradiation is considered 1,000W/m^2, the ambient temperature is 300K, the maximum PV output is 656 W. Thus, all the DC loads (total DC load power is 380 W) with different voltage levels, listed in Table 11, are powered by the PV and the remaining power is delivered to the battery.

 doi:10.20944/preprints202408.0085.v1

Table 11. Constant DC load for case 1.

Voltage level	Load
24 V load	200 W
12 V load	100 W
6 V load	80 W
Total	380 W

At the 1.0 sec, there was a transition in irradiance to 700 W/m², the PV output decreased to 464 W, yet the system continued to operate with a surplus of power. During this period, the battery was charged with an excess power of 84W. Subsequently, at the 2.0s, the irradiance was further reduced to 300 W/m². The PV power output decreased to 198 W, causing the system to enter a power deficit mode. But the dc bus voltage remained steady at 48V throughout the simulation period shown in Figure 22. The deficit power is supplied by the battery with a discharging power around 200 W.

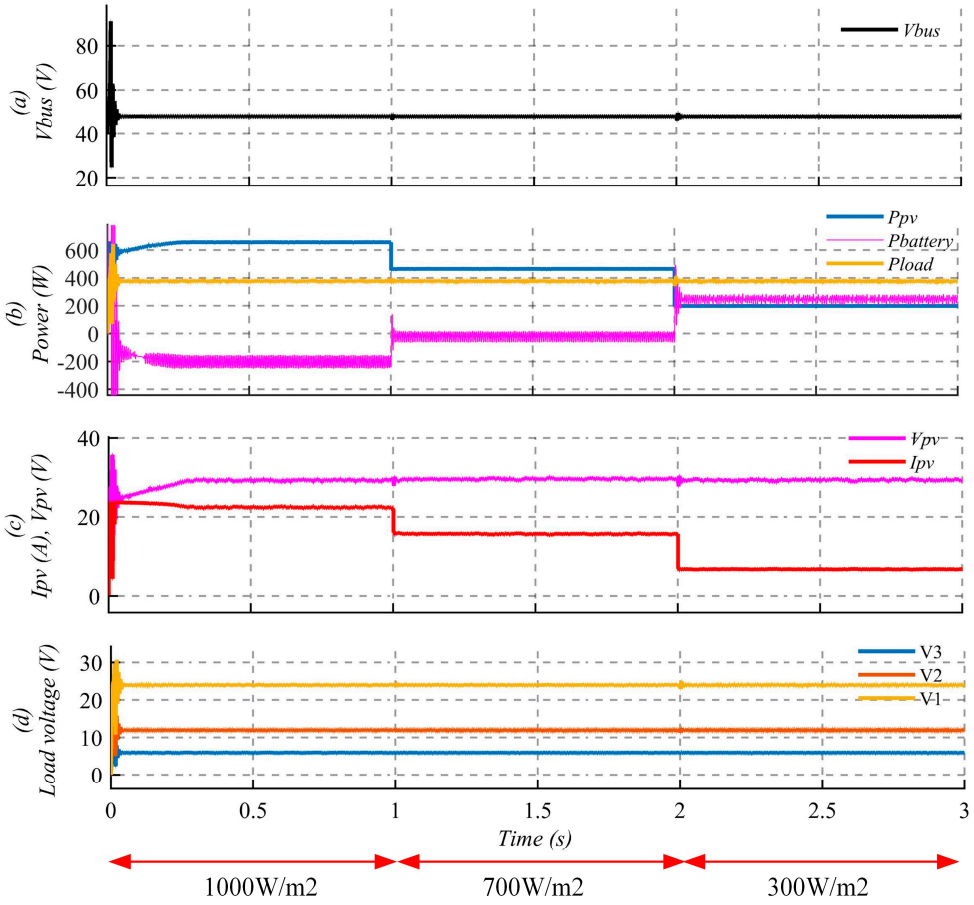

Figure 22. Case 1: PV power variation (a) DC bus voltage, (b) power flow (PV, battery and DC load), (c) PV current and voltage and (d) load voltages.

Case 2: Variation of load

Variation of the total load in the system is the common source of instability in any system. But having tuned PI controllers in the system, the instability is avoided which is already verified in impedance scanning, Now, in the time domain simulation in Figure 23, the DC bus voltage is stable when the DC loads varied according to Table 12. The PV generated power is considered constant throughout the full simulation period at 380W under 500 W/m² irradiance and 300K temperature. Initially the system is in power deficit mode since P_{Load}>P_{PV}. And a slight decrease in DC loads to 400W after 1 second, results in a decrease in power supplied by the battery. The system, however,

 doi:10.20944/preprints202408.0085.v1

remained in power deficit mode. Finally, at 2s the significant decrease in load to 200 W sent the system into power surplus mode and now the system charges the battery with 180W.

Table 12. Variable DC load for case 2.

Voltage level	0-1	1-2	2-3
24 V load	200 W	200 W	200 W
12 V load	200 W	200 W	0 W
6 V load	100 W	0 W	0 W
Total	500 W	400 W	200 W

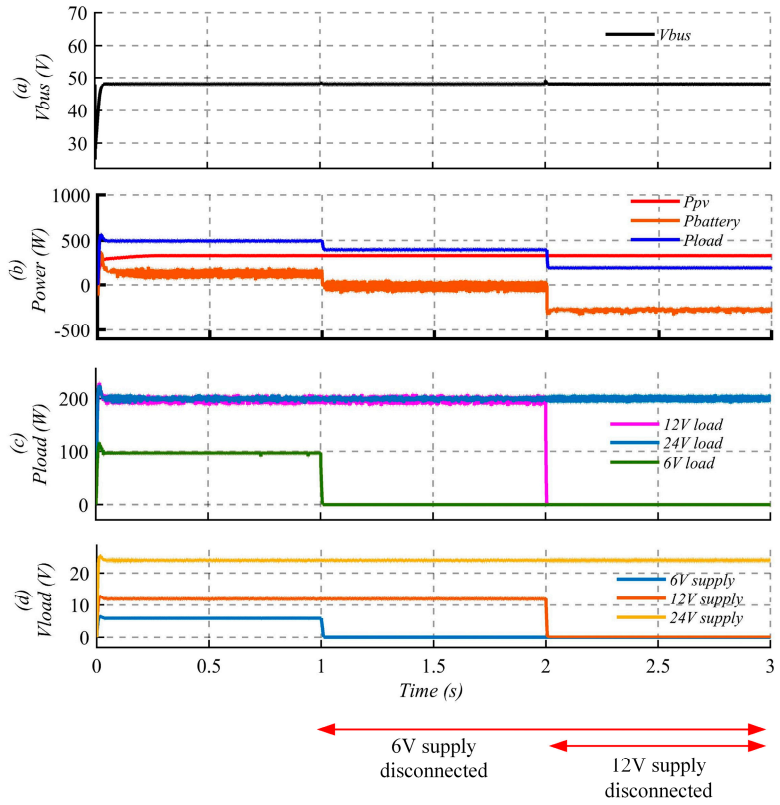

Figure 23. Case 2: PV power variation (a) DC bus voltage, (b) Power flow (PV, battery and DC load), (c) Load power and (d) load voltages.

These two cases and simulation results indicate that the designed nanogrid is stable, and any instability can be mitigated by the converters within the system. To further verify this, the frequency response of the source impedance, load impedance, and total DC bus impedance is analyzed by partitioning the total impedance into output and input impedance elements. The Nyquist plot of the source-to-load impedance ratio is then employed to evaluate the system's stability. Figure 24 presents the Nyquist plot as a function of frequency, demonstrating a significant separation from the (-1,0) point. Consequently, it is evident that the system can be deemed stable.

 doi:10.20944/preprints202408.0085.v1

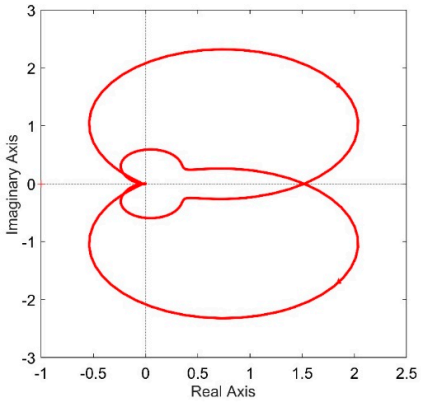

Figure 24. Nyquist plot of total output impedance and input impedance.

3.2. Final Nanogrid Hardware and Validation Tests

The assembled nanogrid hardware is shown in Figure 25. The PV converter, 24V load converter, and battery controller are placed in order from the left, all housed in blue enclosures. The master controller in green encloser is positioned on the far right, close to the Raspberry Pi display.

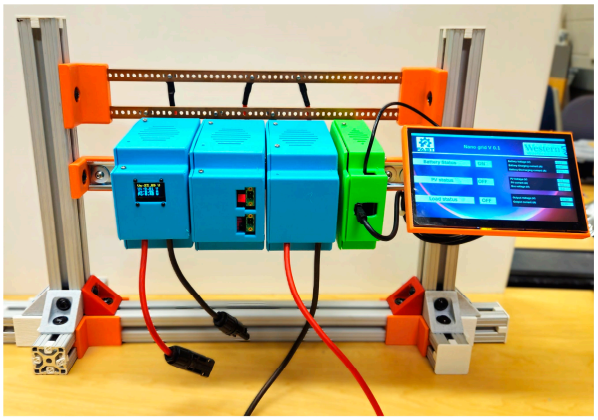

(a)

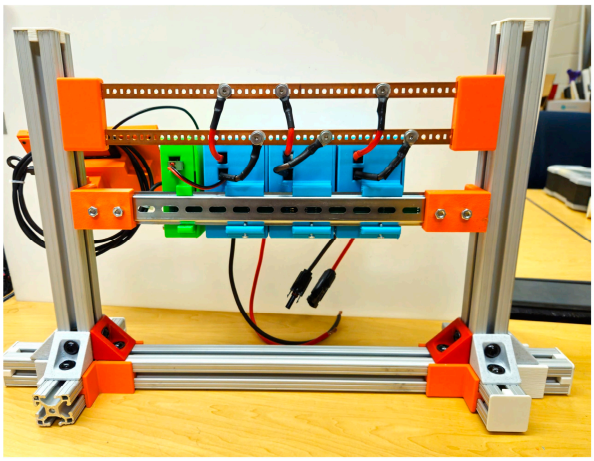

(b)

Figure 25. Nanogrid final hardware (a) front view (b) back view.

 doi:10.20944/preprints202408.0085.v1

3.3. Supply Voltage Stability of 24V Load

A 30W load is connected to the system and subsequently disconnected to evaluate the stability of the supply voltage, as shown in Figure 26. The supply voltage remains stable during the load variation and quickly returns to the reference 24V after the disconnection.

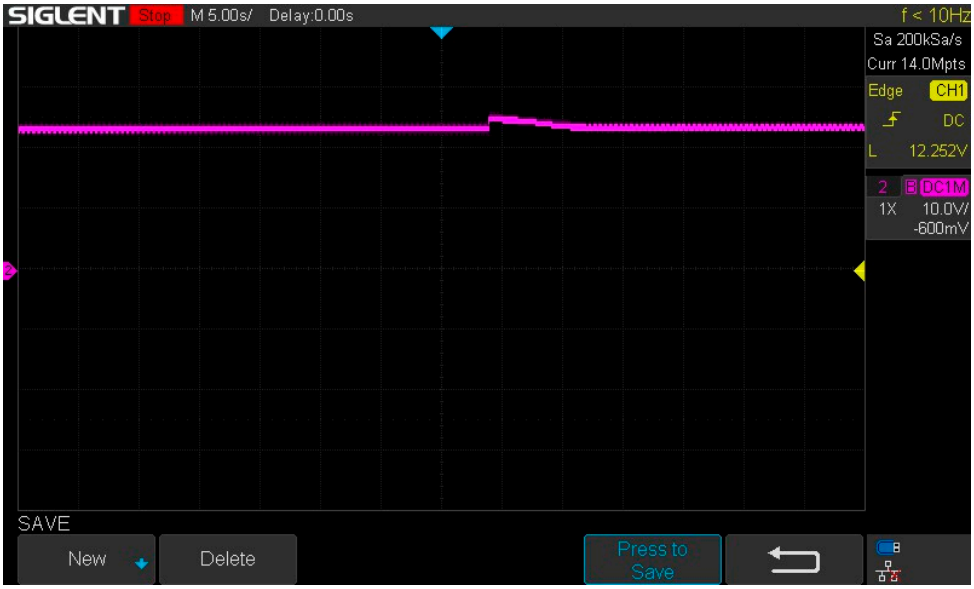

Figure 26. The 24V supply voltage after sudden disconnection of 30W load.

4. Discussion

While hybrid nanogrids can simultaneously provide both AC and DC power [67], the feasibility and benefits of using a DC distribution network in conjunction with renewable energy sources have already been widely explored and documented [68]. Conventional PV systems mostly use inverters to supply AC power to loads, even though most low-power household loads are DC. In contrast, this nanogrid system is entirely DC and can supply power at different DC levels. For a DC nanogrid network, converters play the most significant role in operating the whole system [69]. Therefore, a general design framework for converters was proposed to ensure reliable steady-state and dynamic responses when various loads are integrated into the system [70]. Even to control modern unidirectional and bi-directional DC-DC converters, several control techniques are implemented and discussed briefly [71]. The development of new converter techniques and control mechanisms remains a significant focus for researchers, who are consistently innovating with new control strategies [72] and converter topologies [73] . For instance, experimental validation of a three-port bidirectional converter was conducted, along with a novel control technique, to ensure high reliability when integrated with a solar PV system [74]. Even the interconnection between two DC nanogrid to exchange power and communication between them is demonstrated and explained [75].

This paper differentiates itself by not extensively discussing new control mechanisms or converter designs for DC nanogrids. Instead, it focuses on the comprehensive setup of a DC nanogrid. This includes maximizing power extraction from solar PV, maintaining a stable DC bus voltage, and ensuring the proper operation of the battery system to supply power to appliances at their required voltage levels. A key aspect of its uniqueness is its modularity and the device version of the DC distribution network system. This represents the first-ever nanogrid that incorporates all the features of a complete DC nanogrid in a modular, user-friendly, plug-and-play hardware design. It is designed to be easily assembled and operated by users, making it accessible for DIY applications [76] and enhancing its practicality and flexibility. The hardware implementation is completed using open-source design. Later the bus voltage stability, and the supply voltage quality of the hardware is also

 doi:10.20944/preprints202408.0085.v1

verified. The benefit of the open-source hardware is the adaptation of this nanogrid using material from local vendors and it gives the opportunity to modify the device quite easily according to users' requirements. Its modular design allows for easy integration into a frame or electrical box. Single households, vehicles such as ambulances, mini-clinics, and camps can be powered using the nanogrid setup, with the design facilitating easy modifications to integrate new loads and batteries. While this setup introduces a novel strategy for making PV systems modular and more accessible, further improvements in the GUI and communication system are necessary for the seamless integration of converter modules. Additionally, a better communication strategy is needed to enable the PV converter to share data with the master controller without interruption. Implementing a more advanced MPPT algorithm could also help reduce the impact of partial shading. Currently, the converters are connected to the bus bar using wires, which disrupts seamless integration, but incorporating bus bar clips will make the process easier. Being opensource will allow modifications by the user such as disconnecting low-priority loads when the generation capability is inadequate [77].

5. Conclusions

The open-source modular DC nanogrid presented in this paper represents the first hardware implementation of a plug-and-play device that is, easily adaptable, expandable, and customizable at different voltage and power levels. Transforming the nanogrid from a distribution network to a device makes it suitable for various user-specific applications, such as remotely supplying power to camp vehicles, campsites, emergency vehicles like ambulances, and small houses lacking grid electricity. The modular DC nanogrid includes all the features available in a DC distribution network, including intercommunication of each converter using a master-slave protocol. It also exhibits additional features such as data logging, which enhances user experience and promotes the use of DC grid systems. This approach not only makes the system more user-friendly but also differentiates it from traditional PV systems, promoting the adoption of DC grid systems as a modular device.

The converter technologies, maximum power point tracking (MPPT), and battery charge controller technologies are well-established products which are used on conventional PV systems. The novelty and user-friendly features of the proposed nanogrid system are:

Open-Source Hardware Implementation: Implementing these technologies using open-source hardware and then forming a nanogrid in a modular and adaptable manner is completely novel.

Modular Device Design: Creating the nanogrid as a device with interconnection and control techniques makes it distinct from conventional PV systems.

User-Friendly Features: Additional features such as data logging enhance user experience and promote the use of DC grid systems. This approach not only makes the system more user-friendly but also differentiates it from traditional PV systems, promoting the adoption of DC grid systems.

Author Contributions: Conceptualization, J.M.P.; methodology, M.M.R, S.K., J.M.P.; software, M.M.R..; validation, M.M.R..; formal analysis, M.M.R, S.K., J.M.P.; investigation, M.M.R.; resources, J.M.P.; data curation, M.M.R, S.K., J.M.P.; writing—original draft preparation, M.M.R, S.K., J.M.P.; writing—review and editing, M.M.R, S.K., J.M.P.; visualization, M.M.R, S.K.,; supervision, J.M.P.; project administration, J.M.P.; funding acquisition, J.M.P.. All authors have read and agreed to the published version of the manuscript.

Funding: Please add: This research was funded by the Thompson Endowment and the Natural Sciences and Engineering Research Council of Canada and the Frugal Biomed Initiative at Western University.

Institutional Review Board Statement: Not applicable.

Informed Consent Statement: Not applicable.

Data Availability Statement: All data is available and the design files are at https://osf.io/73yf5/.

Conflicts of Interest: The authors declare no conflicts of interest.". The funders had no role in the design of the study; in the collection, analyses, or interpretation of data; in the writing of the manuscript; or in the decision to publish the results.

 doi:10.20944/preprints202408.0085.v1

Appendix A

The details of the bill of material for each of the modules in the DC nano grid are included here along with designator for the corresponding PCB.

A.1 Buck Converter

Table A1. Bill of material of buck converter.

Designator	Value	Qty	Cost per unit	Total cost	Source of materials
A4	Arduino Nano	1	$10.66	$10.66	https://www.amazon.ca/ELEGOO-Arduino-ATmega328P-Without-Compatible/dp/B0713XK923/?th=1
C1	Cap 470uF, 100V	1	$1.57	$1.57	https://www.digikey.ca/en/products/detail/rubycon/100ZLH470MEFC16X31-5/3564548
C2, C11	Cap 470uF, 50V	2	$0.98	$1.95	https://www.digikey.ca/en/products/detail/nichicon/UPW1H471MHD/589652
C3, C5	Cap .22uF, 50V	1	$0.26	$0.26	https://www.digikey.ca/en/products/detail/nichicon/UVR1HR22MDD/588837
C4	Cap.33uF, 50V	2	$0.26	$0.51	https://www.digikey.ca/en/products/detail/nichicon/UVR2AR33MDD/588879
C6, C7	0.1uF, 0805 SMD	2	$0.04	$0.08	https://www.digikey.ca/en/products/detail/samsung-electro-mechanics/CL21B104KCFNNNE/5961324?
C8	10uF,0805 SMD	1	$0.06	$0.06	https://www.digikey.ca/en/products/detail/samsung-electro-mechanics/CL21A106KOQNNNE/3886754
C9, C10	10nF,0805 SMD	2	$0.10	$0.21	https://www.digikey.ca/en/products/detail/kemet/C0805X103K1RAC3316/10315780
C12	4.7u,0805 SMD	1	$0.06	$0.06	https://www.digikey.ca/en/products/detail/samsung-electro-mechanics/CL21A475KAQNNNE/3886902
C13, C14	2.2u 0805 SMD	1	$0.19	$0.19	https://www.digikey.ca/en/products/detail/samsung-electro-mechanics/CL21B225KAFNFNE/3888611
D1, D2, D3, D4	SS310 0805 SMD	4	$0.74	$2.94	https://www.digikey.ca/en/products/detail/onsemi/S310FA/5892104
F1	Fuse	1	$1.20	$1.20	https://www.digikey.ca/en/products/detail/littelfuse-inc/0997020-WXN/701061
F1	Fuse holder	1	$1.18	$1.18	https://www.digikey.ca/en/products/detail/littelfuse-inc/01000063Z/14641003
J1, J7	Connector 1776508	2	$2.01	$4.02	https://www.digikey.ca/en/products/detail/phoenix-contact/1776508/349000
J3, J6	Screw Terminal	2	$1.07	$2.14	https://www.digikey.ca/en/products/detail/keystone-electronics/8197-2/2746666
J4	JST 4POS2.54MM	1	$0.23	$0.23	https://www.digikey.ca/en/products/detail/jst-sales-america-inc./B4B-XH-A/1651047?
J5	Conn_01x08_Socket	1	$0.29	$0.29	https://www.digikey.ca/en/products/detail/adam-tech/PH1RB-08-UA/9831008?
L1	Inductor Toroidal 0077443A7	1	$7.38	$7.38	https://www.digikey.ca/en/products/detail/magnetics-a-division-of-spang-co/0077443A7/18626894?
Q1, Q2	MOSFET CSD19533KCS	2	$1.71	$3.42	https://www.digikey.ca/en/products/detail/texas-instruments/CSD19533KCS/4806074
R1, R2	47 Ohm 0805	2	$0.02	$0.04	https://www.digikey.ca/en/products/detail/stackpole-electronics-inc/RMCF0805FT47R0/1713163
R3, R4	220 Ohm 0805	2	$0.02	$0.04	https://www.digikey.ca/en/products/detail/stackpole-electronics-inc/RMCF0805FT220R/1760238

 doi:10.20944/preprints202408.0085.v1

R5, R7, R9, R10	100k Ohm 0805	4	$0.02	$0.08	https://www.digikey.ca/en/products/detail/stackpole-electronics-inc/RMCF0805FT100K/1760712
R6, R8	10k Ohm 0805	2	$0.02	$0.04	https://www.digikey.ca/en/products/detail/stackpole-electronics-inc/RMCF0805FT10K0/1760676
U1	MOSFET driver IR2104	1	$5.36	$5.36	https://www.digikey.ca/en/products/detail/infineon-technologies/IR2104PBF/812198
U2	LM7805_TO220	1	$0.79	$0.79	https://www.digikey.ca/en/products/detail/stmicroelectronics/L7805CV/585964
U3	LM7812_TO220	1	$0.98	$0.98	https://www.digikey.ca/en/products/detail/stmicroelectronics/L7812CV/585973
U4	ACS712. 20A	1	$4.29	$4.29	https://www.digikey.ca/en/products/detail/allegro-microsystems/ACS712ELCTR-20A-T/1284607
-	Heat sink	3	$1.17	$3.50	https://www.amazon.ca/Easycargo-Heatsink-Insulator-Regulator-Transistor/dp/B08MW1YNJM/ref=asc_df_B08MW1YNJM/?th=1
-	PCB	1	$2.33	$2.33	https://jlcpcb.com/
			Total	$55.81	

A.2 Boost Converter

Table A2. Bill of material of boost converter.

Designator	Value	Qty	Cost per unit	Total cost	Source of materials
A4	Arduino_Nano_v3.x	1	$10.66	$10.66	https://www.amazon.ca/ELEGOO-Arduino-ATmega328P-Without-Compatible/dp/B0713XK923/?th=1
C1, C18	Cap 470uF, 100V	2	$1.57	$3.15	https://www.digikey.ca/en/products/detail/rubycon/100ZLH470MEFC16X31-5/3564548
C2, C11	Cap 470uF, 50V	2	$0.98	$1.95	https://www.digikey.ca/en/products/detail/nichicon/UPW1H471MHD/589652
C3, C4, C5	Cap .22uF, 50V	3	$0.26	$0.77	https://www.digikey.ca/en/products/detail/nichicon/UVR1HR22MDD/588837
C9, C10	10nF,0805 SMD	2	$0.10	$0.21	https://www.digikey.ca/en/products/detail/kemet/C0805X103K1RAC3316/10315780
C12, C15	4.7u,0805 SMD	2	$0.06	$0.12	https://www.digikey.ca/en/products/detail/samsung-electro-mechanics/CL21A475KAQNNNE/3886902
C13, C17, C14, C16	2.2u 0805 SMD	4	$0.19	$0.77	https://www.digikey.ca/en/products/detail/samsung-electro-mechanics/CL21B225KAFNFNE/3888611
C19	10uF,0805 SMD	1	$0.06	$0.06	https://www.digikey.ca/en/products/detail/samsung-electro-mechanics/CL21A106KOQNNNE/3886754
D2, D3	SS310 0805 SMD	2	$0.74	$1.47	https://www.digikey.ca/en/products/detail/onsemi/S310FA/5892104
D4	APT60S20BG 75A	1	$5.60	$5.60	https://www.digikey.ca/en/products/detail/microchip-technology/APT60S20BG/1494822?
F0	Fuse	1	$1.20	$1.20	https://www.digikey.ca/en/products/detail/littelfuse-inc/0997020-WXN/701061
F1	Fuse holder	1	$1.18	$1.18	https://www.digikey.ca/en/products/detail/littelfuse-inc/01000063Z/14641003

 doi:10.20944/preprints202408.0085.v1

J2, J3, J6, J7	Screw Terminal 8197 2	4	$1.07	$4.28	https://www.digikey.ca/en/products/detail/keystone-electronics/8197-2/2746666
J4	JST 4POS2.54 MM	1	$0.23	$0.23	https://www.digikey.ca/en/products/detail/jst-sales-america-inc./B4B-XH-A/1651047?
J5	Conn_01x08_header	1	$0.29	$0.29	https://www.digikey.ca/en/products/detail/adam-tech/PH1RB-08-UA/9831008?
L1	Inductor toroidal 0077443A7	1	$7.38	$7.38	https://www.digikey.ca/en/products/detail/magnetics-a-division-of-spang-co/0077443A7/18626894?
Q2	MOSFET CSD19533KCS	1	$1.71	$1.71	https://www.digikey.ca/en/products/detail/texas-instruments/CSD19533KCS/4806074
R1, R3, R12, R13, R14, R15	0-ohm, Jumper, 0805	6	$0.01	$0.09	https://www.digikey.ca/en/products/detail/stackpole-electronics-inc/RMCF0805ZT0R00/1756901
R2	47 Ohm 0805 SMD	1	$0.02	$0.02	https://www.digikey.ca/en/products/detail/stackpole-electronics-inc/RMCF0805FT47R0/1713163
R5, R7, R9	100k Ohm 0805 SMD	3	$0.02	$0.06	https://www.digikey.ca/en/products/detail/stackpole-electronics-inc/RMCF0805FT100K/1760712
R6, R8, R11, R16, R17	10k Ohm 0805 SMD	5	$0.02	$0.10	https://www.digikey.ca/en/products/detail/stackpole-electronics-inc/RMCF0805FT10K0/1760676
U2	LM7805CV TO220	1	$0.79	$0.79	https://www.digikey.ca/en/products/detail/stmicroelectronics/L7805CV/585964
U3	LM7812CV TO220	1	$0.98	$0.98	https://www.digikey.ca/en/products/detail/stmicroelectronics/L7812CV/585973
U4, U5	ACS712 20A	2	$4.29	$8.58	https://www.digikey.ca/en/products/detail/allegro-microsystems/ACS712ELCTR-20A-T/1284607
U6	ADS1115IDGSR 16Bit	1	$8.59	$8.59	https://www.digikey.ca/en/products/detail/texas-instruments/ADS1115IDGSR/2231567
-	Heat sink	3	1.17	$3.50	https://www.amazon.ca/Easycargo-Heatsink-Insulator-Regulator-Transistor/dp/B08MW1YNJM/ref=asc_df_B08MW1YNJM/?th=1
-	PCB	1	2.33	2.33	https://jlcpcb.com/
			Total	$66.07	

A.3 Bidirectional Converter

Table A3. Bill of material of Bidirectional converter.

Designator	Value	Qty	Cost per unit	Total cost	Source of materials
A4	Arduino_Nano_v3.x	1	$10.66	$10.66	https://www.amazon.ca/ELEGOO-Arduino-ATmega328P-Without-Compatible/dp/B0713XK923/?th=1
C1, C18	Cap 470uF, 100V	2	$1.57	$3.15	https://www.digikey.ca/en/products/detail/rubycon/100ZLH470MEFC16X31-5/3564548
C2, C11	Cap 470uF, 50V	2	$0.98	$1.95	https://www.digikey.ca/en/products/detail/nichicon/UPW1H471MHD/589652

 doi:10.20944/preprints202408.0085.v1

C3, C4	Cap.33uF, 50V	2	$0.26	$0.51	https://www.digikey.ca/en/products/detail/nichicon/UVR2AR33MDD/588879
C5	Cap .22uF, 50V	1	$0.26	$0.26	https://www.digikey.ca/en/products/detail/nichicon/UVR1HR22MDD/588837
C6, C7	0.1uF, 0805 SMD	2	$0.04	$0.08	https://www.digikey.ca/en/products/detail/samsung-electro-mechanics/CL21B104KCFNNNE/5961324?
C8, C19	10uF,0805 SMD	2	$0.06	$0.12	https://www.digikey.ca/en/products/detail/samsung-electro-mechanics/CL21A106KOQNNNE/3886754
C9, C10	10nF,0805 SMD	2	$0.10	$0.21	https://www.digikey.ca/en/products/detail/kemet/C0805X103K1RAC3316/10315780
C12, C15	4.7uF,0805 SMD	2	$0.06	$0.12	https://www.digikey.ca/en/products/detail/samsung-electro-mechanics/CL21A475KAQNNNE/3886902
C13, C17, C14, C16	2.2uF 0805 SMD	4	$0.19	$0.77	https://www.digikey.ca/en/products/detail/samsung-electro-mechanics/CL21B225KAFNFNE/3888611
D1, D3, D4, D6	SS310 0805 SMD	4	$0.74	$2.94	https://www.digikey.ca/en/products/detail/onsemi/S310FA/5892104
D5	APT60S20BG 75A	1	$5.60	$5.60	https://www.digikey.ca/en/products/detail/microchip-technology/APT60S20BG/1494822?
F1, F2	Fuse	2	$1.20	$2.40	https://www.digikey.ca/en/products/detail/littelfuse-inc/0997020-WXN/701061
J1	Fuse holder	1	$1.18	$1.18	https://www.digikey.ca/en/products/detail/littelfuse-inc/01000063Z/14641003
J2, J3, J6, J7	Screw Terminal 8197 2	4	$1.07	$4.28	https://www.digikey.ca/en/products/detail/keystone-electronics/8197-2/2746666
J4	Screw_Terminal_01x02	1	$0.52	$0.52	https://www.digikey.ca/en/products/detail/cui-devices/TB002-500-02BE/10064069
J5	Conn_01x08_header	1	$0.29	$0.29	https://www.digikey.ca/en/products/detail/adam-tech/PH1RB-08-UA/9831008?
L1	Inductor toroidal 0077443A7	1	$7.38	$7.38	https://www.digikey.ca/en/products/detail/magnetics-a-division-of-spang-co/0077443A7/18626894?
Q1, Q2	MOSFET CSD19533KCS	2	$1.71	$3.42	https://www.digikey.ca/en/products/detail/texas-instruments/CSD19533KCS/4806074
R1, R2	47 Ohm 0805 SMD	2	$0.02	$0.04	https://www.digikey.ca/en/products/detail/stackpole-electronics-inc/RMCF0805FT47R0/1713163
R3, R4, R18	220 Ohm 0805 SMD	2	$0.02	$0.04	https://www.digikey.ca/en/products/detail/stackpole-electronics-inc/RMCF0805FT220R/1760238
R5, R7, R9, R10	100k Ohm 0805 SMD	4	$0.02	$0.08	https://www.digikey.ca/en/products/detail/stackpole-electronics-inc/RMCF0805FT100K/1760712
R6, R8, R11, R16, R17	10k Ohm 0805 SMD	5	$0.02	$0.10	https://www.digikey.ca/en/products/detail/stackpole-electronics-inc/RMCF0805FT10K0/1760676
R12, R13, R14, R15	0-ohm, Jumper, 0805	4	$0.01	$0.06	https://www.digikey.ca/en/products/detail/stackpole-electronics-inc/RMCF0805ZT0R00/1756901
U1	MOSFET driver IR2104	1	$5.36	$5.36	https://www.digikey.ca/en/products/detail/infineon-technologies/IR2104PBF/812198
U2	LM7805CV TO220	1	$0.79	$0.79	https://www.digikey.ca/en/products/detail/stmicroelectronics/L7805CV/585964
U3	LM7812CV TO220	1	$0.98	$0.98	https://www.digikey.ca/en/products/detail/stmicroelectronics/L7812CV/585973
U4, U5	ACS712 20A	2	$4.29	$8.58	https://www.digikey.ca/en/products/detail/allegro-microsystems/ACS712ELCTR-20A-T/1284607

 doi:10.20944/preprints202408.0085.v1

U6	ADS1115IDGSR 16Bit	1	$8.59	$8.59	https://www.digikey.ca/en/products/detail/texas-instruments/ADS1115IDGSR/2231567
-	Heat sink	3	$1.17	$3.50	https://www.amazon.ca/Easycargo-Heatsink-Insulator-Regulator-Transistor/dp/B08MW1YNJM/ref=asc_df_B08MW1YNJM/?th=1
-	PCB	1	$2.33	$2.33	https://jlcpcb.com/
			Total	$76.28	

A.4 Master Controller

Table A4. Bill of material of Master Controller.

Designator	Value	Qnty	Cost per unit	Total cost	Source of materials
A4	Arduino_Nano_v3.x	1	$10.66	$10.66	https://www.amazon.ca/ELEGOO-Arduino-ATmega328P-Without-Compatible/dp/B0713XK923/?th=1
C4, C5	.22uF	2	$0.26	$0.51	https://www.digikey.ca/en/products/detail/nichicon/UVR1HR22MDD/588837
D2	SS310 0805 SMD	1	$0.74	$0.74	https://www.digikey.ca/en/products/detail/onsemi/S310FA/5892104
J1, J3	JST 4POS2.54MM	2	$0.23	$0.46	https://www.digikey.ca/en/products/detail/jst-sales-america-inc./B4B-XH-A/1651047?
J2, J4	Screw_Terminal_01x02	1	$0.52	$0.52	https://www.digikey.ca/en/products/detail/cui-devices/TB002-500-02BE/10064069
J5	Conn_01x08 Pin header	1	$0.29	$0.29	https://www.digikey.ca/en/products/detail/adam-tech/PH1RB-08-UA/9831008?
J6, J7	Conn_01x06_Socket	2			
R3, R4	10k Ohm 0805 SMD	2	$0.02	$0.04	https://www.digikey.ca/en/products/detail/stackpole-electronics-inc/RMCF0805FT10K0/1760676
R1, R2	220 Ohm 0805 SMD	2	$0.02	$0.04	https://www.digikey.ca/en/products/detail/stackpole-electronics-inc/RMCF0805FT220R/1760238
U2	LM7805CV TO220	1	$0.79	$0.79	https://www.digikey.ca/en/products/detail/stmicroelectronics/L7805CV/585964
-	Heat sink	3	$1.17	$3.50	https://www.amazon.ca/Easycargo-Heatsink-Insulator-Regulator-Transistor/dp/B08MW1YNJM/ref=asc_df_B08MW1YNJM/?th=1
-	15W Converter for pi	1	$8.90	$8.90	https://www.amazon.ca/DKARDU-Converter-Voltage-Regulator-Charger/dp/B0B2RF1L92/
-	PCB	1	$2.33	$2.33	https://jlcpcb.com/
			Total	$28.78	

 doi:10.20944/preprints202408.0085.v1

A.5 Communication Bus

Table A5. Bill of material of communication bus.

Designator	Value	Qnty	Cost per unit	Total cost	Source of materials
J2, J3, J4, J6	Conn_01x08_Socket	4	$0.41	$1.64	https://www.digikey.ca/en/products/detail/w%C3%BCrth-elektronik/61300811821/17737805?
J1,	Conn_01x08_Socket vertical	1	$0.77	$0.77	https://www.digikey.ca/en/products/detail/sullins-connector-solutions/PPPC081LGBN-RC/775941?
J7	Conn_01x08 Pin Right angle	1	$0.29	$0.29	https://www.digikey.ca/en/products/detail/adam-tech/PH1RB-08-UA/9831008?
-	PCB	1	$2.33	$2.33	https://jlcpcb.com/
			Total	$5.03	

A.6 Data Monitoring and Logging System

Table A6. Bill of material of monitoring system.

Component	Qnty	Cost per unit	Total cost	Source of materials
Raspberry Pi	1	$45.00	$45.00	https://www.digikey.ca/en/products/detail/raspberry-pi/SC0193(9)/10258782?
7-inch touch screen	1	$63.95	$63.95	https://www.amazon.ca/dp/B0B44VZTRG/
DIN rail	1	$7.26	$7.26	https://www.digikey.ca/en/products/detail/altech-corporation/2511120%2F1M/8546913?
Bus bar	1	$31.31	$31.31	https://www.digikey.ca/en/products/detail/weidm%C3%BCller/0280300000/491744?
		Total	$147.52	

References

1. Zhou, X.; Guo, T.; Ma, Y. An Overview on Microgrid Technology. In Proceedings of the 2015 IEEE International Conference on Mechatronics and Automation (ICMA); August 2015; pp. 76–81.
2. Nordman, B.; Christensen, K. DC Local Power Distribution with Microgrids and Nanogrids. In Proceedings of the 2015 IEEE First International Conference on DC Microgrids (ICDCM); June 2015; pp. 199–204.
3. Schonbergerschonberger, J.; Duke, R.; Round, S.D. DC-Bus Signaling: A Distributed Control Strategy for a Hybrid Renewable Nanogrid. *IEEE Transactions on Industrial Electronics* **2006**, *53*, 1453–1460, doi:10.1109/TIE.2006.882012.
4. Nag, S.; Adda, R.; Ray, O.; Mishra, S. Current-Fed Switched Inverter Based Hybrid Topology for DC Nanogrid Application; 2013; p. 7151;.
5. Pearce, J.M. Photovoltaics — a Path to Sustainable Futures. *Futures* **2002**, *34*, 663–674, doi:10.1016/S0016-3287(02)00008-3.
6. Tsuma, M.; Kibaara, S. A Review of Levelized Cost of Electricity for Photovoltaic Systems Combining with Their Environmental Impacts. *Proceedings of the Sustainable Research and Innovation Conference* **2022**, 220–225.
7. Zhang, P.; Li, W.; Li, S.; Wang, Y.; Xiao, W. Reliability Assessment of Photovoltaic Power Systems: Review of Current Status and Future Perspectives. *Applied Energy* **2013**, *104*, 822–833, doi:10.1016/j.apenergy.2012.12.010.
8. Şen, Z. Solar Energy in Progress and Future Research Trends. *Progress in Energy and Combustion Science* **2004**, *30*, 367–416, doi:10.1016/j.pecs.2004.02.004.

 doi:10.20944/preprints202408.0085.v1

9. Vives, M.V.; Chamorro, H.R.; Ortiz-Villalba, D.; Jiménez, F.; Gonzalez-Longatt, F.M.; Jimenez-Estevez, G.; Guerrero, J.; Cadena, A.; Sood, V.K. Nanogrids: Good Practices and Challenges in the Projects in Colombia. In *Microgrids for Rural Areas*; Institution of Engineering and Technology, 2020; pp. 421–446.
10. Assis, F.A.; Coelho, F.C.R.; Castro, J.F.C.; Donadon, A.R.; Roncolatto, R.A.; Rosas, P.A.C.; Andrade, V.E.M.S.; Bento, R.G.; Silva, L.C.P.; Cypriano, J.G.I.; et al. Assessment of Regulatory and Market Challenges in the Economic Feasibility of a Nanogrid: A Brazilian Case. *Energies* **2024**, *17*, 341, doi:10.3390/en17020341.
11. Breyer, C. Low-Cost Solar Power Enables a Sustainable Energy Industry System. *Proceedings of the National Academy of Sciences* **2021**, *118*, e2116940118, doi:10.1073/pnas.2116940118.
12. Staff, C.B. Solar Is Now 'Cheapest Electricity in History', Confirms IEA Available online: https://www.carbonbrief.org/solar-is-now-cheapest-electricity-in-history-confirms-iea/ (accessed on 28 July 2024).
13. Sajeeb, M.M.H.; Rahman, A.; Arif, S. Feasibility Analysis of Solar DC Nano Grid for off Grid Rural Bangladesh. In Proceedings of the 2015 3rd International Conference on Green Energy and Technology (ICGET); September 2015; pp. 1–5.
14. Khan, M.R.; Brown, E.D. DC Nanogrids: A Low Cost PV Based Solution for Livelihood Enhancement for Rural Bangladesh. In Proceedings of the 2014 3rd International Conference on the Developments in Renewable Energy Technology (ICDRET); May 2014; pp. 1–5.
15. Hamatwi, E.; Davidson, I.E.; Agee, J.; Venayagamoorthy, G. Model of a Hybrid Distributed Generation System for a DC Nano-Grid. In Proceedings of the 2016 Clemson University Power Systems Conference (PSC); March 2016; pp. 1–8.
16. Dahiru, A.T.; Tan, C.W. Optimal Sizing and Techno-Economic Analysis of Grid-Connected Nanogrid for Tropical Climates of the Savannah. *Sustainable Cities and Society* **2020**, *52*, 101824, doi:10.1016/j.scs.2019.101824.
17. Shwehdi, M.H.; Mohamed, S.R. Proposed Smart DC Nano-Grid for Green Buildings — A Reflective View. In Proceedings of the 2014 International Conference on Renewable Energy Research and Application (ICRERA); October 2014; pp. 765–769.
18. Mishra, S.; Ray, O. Advances in Nanogrid Technology and Its Integration into Rural Electrification in India. In Proceedings of the 2014 International Power Electronics Conference (IPEC-Hiroshima 2014 - ECCE ASIA); May 2014; pp. 2707–2713.
19. Kinn, M.C. Proposed Components for the Design of a Smart Nano-Grid for a Domestic Electrical System That Operates at below 50V DC. In Proceedings of the 2011 2nd IEEE PES International Conference and Exhibition on Innovative Smart Grid Technologies; December 2011; pp. 1–7.
20. Taufik, T.; Muscarella, M. Development of DC House Prototypes as Demonstration Sites for an Alternate Solution to Rural Electrification. In Proceedings of the 2016 6th International Annual Engineering Seminar (InAES); August 2016; pp. 262–265.
21. Khan, S.; Rahman, Md.M. Design and Simulation of Solar DC Nano Grid System from Bangladesh Perspective. In Proceedings of the 2021 International Conference on Automation, Control and Mechatronics for Industry 4.0 (ACMI); July 2021; pp. 1–6.
22. Joseph, S.C.; Ashok, S.; Dhanesh, P.R. Low Voltage Direct Current(LVDC) Nanogrid for Home Application. In Proceedings of the 2017 IEEE Region 10 Symposium (TENSYMP); July 2017; pp. 1–5.
23. Tudu, B.; Mandal, K.K.; Chakraborty, N. Optimal Design and Development of PV-Wind-Battery Based Nano-Grid System: A Field-on-Laboratory Demonstration. *Front. Energy* **2019**, *13*, 269–283, doi:10.1007/s11708-018-0573-z.
24. Almasri, A.; Al Shabrawi, B.; Sardar, A.; Al Atifi, A.; Al Harbi, A.; Ammous, A. Contribution to the Realization of DC Nano-Grid Including PV Source. In Proceedings of the 2020 Industrial & Systems Engineering Conference (ISEC); July 2020; pp. 1–5.
25. Cvetkovic, I.; Dong, D.; Zhang, W.; Jiang, L.; Boroyevich, D.; Lee, F.C.; Mattavelli, P. A Testbed for Experimental Validation of a Low-Voltage DC Nanogrid for Buildings. In Proceedings of the 2012 15th International Power Electronics and Motion Control Conference (EPE/PEMC); September 2012; p. LS7c.5-1-LS7c.5-8.
26. Rahman, M.M.; Antonini, G.; Pearce, J. Open-Source DC-DC Converter Enabling Direct Integration of Solar Photovoltaics with Anion Exchange Membrane Electrolyzer for Green Hydrogen Production 2024.
27. Gadzanku, S.; Kramer, A.; Smith, B. An Updated Review of the Solar PV Installation Workforce Literature. **2023**, doi:10.2172/1971876.

28. Chagas, A.M. Haves and Have Nots Must Find a Better Way: The Case for Open Scientific Hardware. *PLOS Biology 16*, p.e3000014.
29. Gibb, A. Building Open Source Hardware: DIY Manufacturing for Hackers and Makers; Addison-Wesley Professional, 2014; ISBN 978-0-13-337390-5.
30. Rahman, M.M.; Pearce, J. Modular Open Source Solar Photovoltaic-Powered DC Nanogrids with Efficient Energy Management System. *Solar Energy and Sustainable Development Journal* **2024**, *13*, 22–42, doi:10.51646/jsesd.v13i1.169.
31. Dong, D.; Cvetkovic, I.; Boroyevich, D.; Zhang, W.; Wang, R.; Mattavelli, P. Grid-Interface Bidirectional Converter for Residential DC Distribution Systems—Part One: High-Density Two-Stage Topology. *IEEE Transactions on Power Electronics* **2013**, *28*, 1655–1666, doi:10.1109/TPEL.2012.2212462.
32. Sudev, V.; Parvathy, S. Switched Boost Inverter Based Dc Nanogrid with Battery and Bi-Directional Converter. In Proceedings of the 2014 International Conference on Circuits, Power and Computing Technologies [ICCPCT-2014]; March 2014; pp. 461–467.
33. Ganesan, S.I.; Pattabiraman, D.; Govindarajan, R.K.; Rajan, M.; Nagamani, C. Control Scheme for a Bidirectional Converter in a Self-Sustaining Low-Voltage DC Nanogrid. *IEEE Transactions on Industrial Electronics* **2015**, *62*, 6317–6326, doi:10.1109/TIE.2015.2424192.
34. Sathler, H.H.; Sathler, L.H.; Marcelino, F.L.F.; de Oliveira, T.R.; Seleme, S.I.; Garcia, P.F.D. A Comparative Efficiency Study on Bidirectional Grid Interface Converters Applied to Low Power DC Nanogrids. In Proceedings of the 2017 Brazilian Power Electronics Conference (COBEP); November 2017; pp. 1–6.
35. Queiroz, F.; Praça, P.; Freitas, A.; Antunes, F. High-Gain Bidirectional DC-DC Converter for Battery Charging in DC Nanogrid of Residential Prossumer. In Proceedings of the 2019 IEEE 15th Brazilian Power Electronics Conference and 5th IEEE Southern Power Electronics Conference (COBEP/SPEC); December 2019; pp. 1–6.
36. Goud, P.C.D.; Gupta, R. Solar PV Based Nanogrid Integrated with Battery Energy Storage to Supply Hybrid Residential Loads Using Single-Stage Hybrid Converter. *IET Energy Systems Integration* **2020**, *2*, 161–169, doi:10.1049/iet-esi.2019.0030.
37. Saxena, A.R.; Kulshreshtha, A. A Fourth-Order Bidirectional DC–DC Converter for Interfacing Battery in a Solar -Photovoltaic-Fed Low-Voltage Residential DC Nano-Grid: Design and Analysis. *International Journal of Circuit Theory and Applications* **2021**, *49*, 1932–1958, doi:10.1002/cta.3016.
38. Bodele, N.J.; Kulkarni, P.S. Modular Battery-Integrated Bidirectional Single-Stage DC–DC Converter for Solar PV Based DC Nano-Grid Application. *Solar Energy* **2023**, *259*, 1–14, doi:10.1016/j.solener.2023.04.040.
39. Burmester, D.; Rayudu, R.; Seah, W.; Akinyele, D. A Review of Nanogrid Topologies and Technologies. *Renewable and Sustainable Energy Reviews* **2017**, *67*, 760–775, doi:10.1016/j.rser.2016.09.073.
40. Controlled Power Sequencing for Fault Protection in DC Nanogrids | IEEE Conference Publication | IEEE Xplore Available online: https://ieeexplore.ieee.org/document/6036384 (accessed on 21 July 2024).
41. Sadabadi, M.S.; Karimi, A.; Karimi, H. Fixed-Order Decentralized/Distributed Control of Islanded Inverter-Interfaced Microgrids. *Control Engineering Practice* **2015**, *45*, 174–193, doi:10.1016/j.conengprac.2015.09.003.
42. Uddin, M.; Mo, H.; Dong, D.; Elsawah, S.; Zhu, J.; Guerrero, J.M. Microgrids: A Review, Outstanding Issues and Future Trends. *Energy Strategy Reviews* **2023**, *49*, 101127, doi:10.1016/j.esr.2023.101127.
43. Oberloier, S.; Whisman, N.G.; Hafting, F.; Pearce, J.M. Open Source Framework for a Broadly Expandable and Reconfigurable Data Acquisition and Automation Device (BREAD). *HardwareX* **2023**, *15*, e00467, doi:10.1016/j.ohx.2023.e00467.
44. Schmid, F.; Behrendt, F. Optimal Sizing of Solar Home Systems: Charge Controller Technology and Its Influence on System Design. *Sustainable Energy Technologies and Assessments* **2021**, *45*, 101198, doi:10.1016/j.seta.2021.101198.
45. Pearce, J.M. Open-Source Lab: How to Build Your Own Hardware and Reduce Research Costs; Elsevier, 2013; ISBN 978-0-12-410486-0.
46. Pearce, J.M. Cut Costs with Open-Source Hardware. *Nature* **2014**, *505*, 618–618, doi:10.1038/505618d.
47. Buitenhuis, A.J.; Pearce, J.M. Open-Source Development of Solar Photovoltaic Technology. *Energy for Sustainable Development* **2012**, *16*, 379–388, doi:10.1016/j.esd.2012.06.006.
48. de Arquer Fernández, P.; Fernández Fernández, M.Á.; Carús Candás, J.L.; Arboleya Arboleya, P. An IoT Open Source Platform for Photovoltaic Plants Supervision. *International Journal of Electrical Power & Energy Systems* **2021**, *125*, 106540, doi:10.1016/j.ijepes.2020.106540.

49. González, I.; Portalo, J.M.; Calderón, A.J. Configurable IoT Open-Source Hardware and Software I-V Curve Tracer for Photovoltaic Generators. *Sensors* **2021**, *21*, 7650, doi:10.3390/s21227650.
50. Portalo, J.M.; González, I.; Calderón, A.J. Monitoring System for Tracking a PV Generator in an Experimental Smart Microgrid: An Open-Source Solution. *Sustainability* **2021**, *13*, 8182, doi:10.3390/su13158182.
51. Santhosh, R.; Sabareesh, S.U.; Aswin, R.; Mahalakshmi, R. Hardware Design of PIC Microcontroller Based Charge Controller and MPPT for the Standalone PV-Battery Charging System. In Proceedings of the 2021 International Conference on Recent Trends on Electronics, Information, Communication & Technology (RTEICT); August 2021; pp. 172–175.
52. Parandhaman, M.; Annambhotla, L.T.S.; Parthiban, P. Hardware Prototype for Portable Automatic MPPT Solar Charger Using Buck Converter and PSO Technique. In Proceedings of the 2022 IEEE Delhi Section Conference (DELCON); February 2022; pp. 1–6.
53. Design of Maximum Power Point Tracking Photovoltaic System Based on Incremental Conductance Algorithm Using Arduino Uno and Boost Converter. *Applied Technology and Computing Science Journal* **2022**, *4*, 101–112, doi:https://doi.org/10.33086/atcsj.v4i2.2450.
54. Podder, A.K.; Roy, N.K.; Pota, H.R. MPPT Methods for Solar PV Systems: A Critical Review Based on Tracking Nature. *IET Renewable Power Generation* **2019**, *13*, 1615–1632, doi:10.1049/iet-rpg.2018.5946.
55. Fangrui Liu; Shanxu Duan; Fei Liu; Bangyin Liu; Yong Kang A Variable Step Size INC MPPT Method for PV Systems. *IEEE Trans. Ind. Electron.* **2008**, *55*, 2622–2628, doi:10.1109/TIE.2008.920550.
56. Karami, N.; Moubayed, N.; Outbib, R. General Review and Classification of Different MPPT Techniques. *Renewable and Sustainable Energy Reviews* **2017**, *68*, 1–18, doi:10.1016/j.rser.2016.09.132.
57. Rahman, Md.M.; Islam, M.S. Artificial Neural Network Based Maximum Power Point Tracking of a Photovoltaic System. In Proceedings of the 2019 3rd International Conference on Electrical, Computer & Telecommunication Engineering (ICECTE); December 2019; pp. 117–120.
58. Rahman, Md.M.; Islam, Md.S. PSO and ANN Based Hybrid MPPT Algorithm for Photovoltaic Array under Partial Shading Condition. *Eng. int. (Dhaka)* **2020**, *8*, 9–24, doi:10.18034/ei.v8i1.481.
59. Mohapatra, A.; Nayak, B.; Das, P.; Mohanty, K.B. A Review on MPPT Techniques of PV System under Partial Shading Condition. *Renewable and Sustainable Energy Reviews* **2017**, *80*, 854–867, doi:10.1016/j.rser.2017.05.083.
60. Yaichi, M.; Fellah, M.-K.; Mammeri, A. A Neural Network Based MPPT Technique Controller for Photovoltaic Pumping System. *International Journal of Power Electronics and Drive Systems (IJPEDS)* **2014**, *4*, 241–255.
61. Yap, K.Y.; Sarimuthu, C.R.; Lim, J.M.-Y. Artificial Intelligence Based MPPT Techniques for Solar Power System: A Review. *Journal of Modern Power Systems and Clean Energy* **2020**, *8*, 1043–1059, doi:10.35833/MPCE.2020.000159.
62. Katche, M.L.; Makokha, A.B.; Zachary, S.O.; Adaramola, M.S. A Comprehensive Review of Maximum Power Point Tracking (MPPT) Techniques Used in Solar PV Systems. *Energies* **2023**, *16*, 2206, doi:10.3390/en16052206.
63. Rahman, M.M.; Khan, S.; Pearce, J.M. Open Source Modular DC Nano Grid Hardware Designs Available online: https://osf.io/73yf5/ (accessed on 23 July 2024).
64. CSD19533KCS Data Sheet, Product Information and Support | TI.Com Available online: https://www.ti.com/product/CSD19533KCS? (accessed on 24 July 2024).
65. Jones, R.; Haufe, P.; Sells, E.; Iravani, P.; Olliver, V.; Palmer, C.; Bowyer, A. RepRap – the Replicating Rapid Prototyper. *Robotica* **2011**, *29*, 177–191, doi:10.1017/S026357471000069X.
66. Sells, E.; Bailard, S.; Smith, Z.; Bowyer, A.; Olliver, V. RepRap: The Replicating Rapid Prototyper: Maximizing Customizability by Breeding the Means of Production. In *Handbook of Research in Mass Customization and Personalization*; World Scientific Publishing Company, 2009; pp. 568–580 ISBN 978-981-4280-25-9.
67. Chandrasena, R.; Shahnia, F.; Ghosh, A.; Rajakaruna, S. Operation and Control of a Hybrid AC-DC Nanogrid for Future Community Houses; 2014;
68. Justo, J.J.; Mwasilu, F.; Lee, J.; Jung, J.-W. AC-Microgrids versus DC-Microgrids with Distributed Energy Resources: A Review. *Renewable and Sustainable Energy Reviews* **2013**, *24*, 387–405, doi:10.1016/j.rser.2013.03.067.

69. Qu, D.; Wang, M.; Sun, Z.; Chen, G. An Improved DC-Bus Signaling Control Method in a Distributed Nanogrid Interfacing Modular Converters. In Proceedings of the 2015 IEEE 11th International Conference on Power Electronics and Drive Systems; June 2015; pp. 214–218.
70. Martin, K.; Vázquez, A.; Arias, M.; Sebastián, J. Optimization Procedure of Source/Sink Converters for DC Power Distribution Nano-Grids. In Proceedings of the 2018 IEEE 19th Workshop on Control and Modeling for Power Electronics (COMPEL); June 2018; pp. 1–8.
71. Ganguly, A.; Biswas, P.K.; Sain, C.; Ustun, T.S. Modern DC–DC Power Converter Topologies and Hybrid Control Strategies for Maximum Power Output in Sustainable Nanogrids and Picogrids—A Comprehensive Survey. *Technologies* **2023**, *11*, 102, doi:10.3390/technologies11040102.
72. Nguyen, T.; Guerrero, J.; Griepentrog, G. A Self-Sustained and Flexible Control Strategy for Islanded DC Nanogrids Without Communication Links. *IEEE Journal of Emerging and Selected Topics in Power Electronics* **2019**, *PP*, 1–1, doi:10.1109/JESTPE.2019.2894564.
73. Fares, A.M.; Klumpner, C.; Sumner, M. A Novel Modular Multiport Converter for Enhancing the Performance of Photovoltaic-Battery Based Power Systems. *Applied Sciences* **2019**, *9*, 3948, doi:10.3390/app9193948.
74. Askarian, I.; Pahlevani, M.; Knight, A.M. Three-Port Bidirectional DC/DC Converter for DC Nanogrids. *IEEE Transactions on Power Electronics* **2021**, *36*, 8000–8011, doi:10.1109/TPEL.2020.3046453.
75. Werth, A.; Kitamura, N.; Tanaka, K. Conceptual Study for Open Energy Systems: Distributed Energy Network Using Interconnected DC Nanogrids. *IEEE Transactions on Smart Grid* **2015**, *6*, 1621–1630, doi:10.1109/TSG.2015.2408603.
76. Grafman, L.; Pearce, J.M.; Droz, P.; Louie, H. To Catch the Sun: Inspiring Stories of Communities Coming Together to Harness Their Own Solar Energy, and How You Can Do It Too!; Humboldt State University Press: Arcata, 2021; ISBN 978-1-947112-62-9.
77. Kalair, A.R.; Abas, N.; Hasan, Q.U.; Seyedmahmoudian, M.; Khan, N. Demand Side Management in Hybrid Rooftop Photovoltaic Integrated Smart Nano Grid. *Journal of Cleaner Production* **2020**, *258*, 120747, doi:10.1016/j.jclepro.2020.120747.